

See discussions, stats, and author profiles for this publication at: <https://www.researchgate.net/publication/323625674>

Stabilized backward in time explicit marching schemes in the numerical computation of ill-posed time-reversed hyperbolic/parabolic systems

Article in *Inverse Problems in Science and Engineering* · March 2018

DOI: 10.1080/17415977.2018.1446952

CITATIONS

2

READS

79

1 author:



Alfred Carasso

National Institute of Standards and Technology

66 PUBLICATIONS 1,100 CITATIONS

SEE PROFILE

STABILIZED BACKWARD IN TIME EXPLICIT MARCHING SCHEMES IN THE NUMERICAL COMPUTATION OF ILL-POSED TIME-REVERSED HYPERBOLIC/PARABOLIC SYSTEMS

ALFRED S. CARASSO*

Abstract. This paper develops stabilized explicit marching difference schemes that can successfully solve a significant but *limited* class of multidimensional, ill-posed, backward in time problems for coupled hyperbolic/parabolic systems associated with vibrating thermoelastic plates and coupled sound and heat flow. Stabilization is achieved by applying compensating smoothing operators at each time step, to quench the instability. Analysis of convergence is restricted to the transparent case of linear, autonomous, selfadjoint spatial differential operators, and *almost best-possible* error bounds are obtained for backward in time reconstruction in that class of problems. However, the actual computational schemes can be applied to more general problems, including examples with variable time dependent coefficients, as well as nonlinearities.

The stabilized explicit schemes are unconditionally stable, marching forward or backward in time, but the smoothing operation at each step leads to a distortion away from the true solution. This is the *stabilization penalty*. It is shown that in many problems of interest, that distortion is small enough to allow for useful results.

Backward in time continuation is illustrated using 512×512 pixel images. Such images are associated with highly irregular non smooth intensity data that severely challenge ill-posed reconstruction procedures. Several computational experiments show that efficient FFT-synthesized smoothing operators, based on $(-\Delta)^p$ with real $p > 2$, can be successfully applied in a broad range of problems.

Key words. thermoelastic systems backward in time; coupled sound and heat flow backward in time; stabilized explicit marching schemes; error bounds; numerical experiments.

AMS subject classifications. 35L15, 35K15, 35R25, 65N12, 65N21.

1. Introduction. Continuing a line of work developed in [1–3], this paper constructs stabilized explicit marching difference schemes that can successfully solve a significant but *limited* class of multidimensional, ill-posed, backward in time problems, for coupled hyperbolic/parabolic equations associated with vibrating thermoelastic plates and coupled sound and heat flow. Stabilization is achieved by applying compensating smoothing operators at each time step, to quench the instability. Analysis of convergence is restricted to the transparent case of linear, autonomous, selfadjoint spatial differential operators, and *almost best-possible* error bounds are obtained for backward in time reconstruction in that class of problems. However, the actual computational schemes can be applied to more general problems, including examples with variable time dependent coefficients, as well as nonlinearities. Instructive computational experiments illustrate the fact that efficient FFT-synthesized smoothing operators, based on $(-\Delta)^p$ with real $p > 2$, can be successfully applied even in some nonlinear backward problems defined in non-rectangular regions.

The paper is organized as follows. In Section 2, an explicit example highlights the inherent uncertainty in backward reconstruction from noisy data. In Section 3, a stable explicit marching scheme is constructed for the thermoelastic plate initial value problem. In Section 4, Theorems 1 and 2 establish error estimates for the forward and backward explicit schemes. These estimates delineate the class of problems wherein the explicit scheme may be useful. Section 5 describes an instructive computational experiment on backward reconstruction in the linear thermoelastic problem. Section 6 discusses the use of smoothing operators based on the Laplacian, even in problems

*Applied and Computational Mathematics Division, National Institute of Standards and Technology, Gaithersburg, MD 20899. (alfred.carasso@nist.gov).

IMAGES ARE DEFINED BY HIGHLY NON SMOOTH INTENSITY DATA THAT CHALLENGE ILL-POSED RECOVERY METHODS

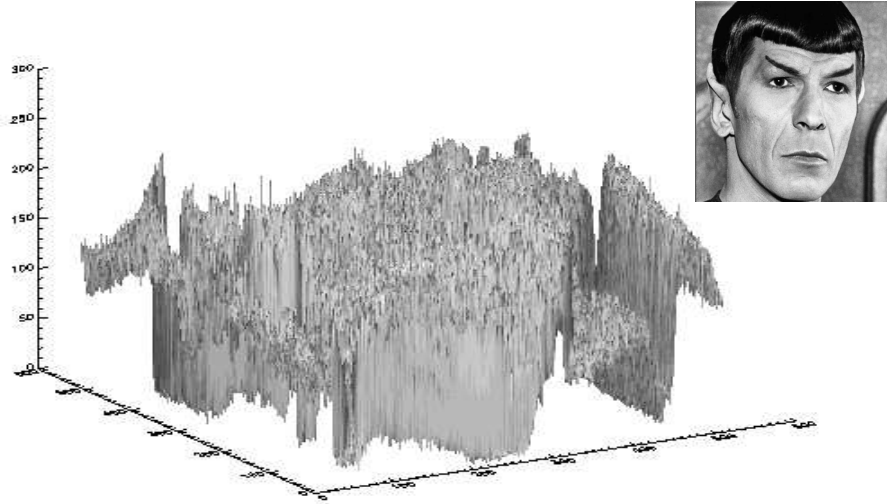


FIG. 1.1. Plot of intensity values $u(x,y)$ versus (x,y) in 512×512 pixel Mr Spock image. Intensity values range from 0 to 255, and result in highly non smooth surface. Such images provide excellent test examples for ill-posed reconstruction methods.

where the second order elliptic spatial differential operator L has variable coefficients. Section 7 describes a backward reconstruction experiment on a nonlinear thermoelastic problem lying outside the scope of the theory discussed in Sections 3 to 6. Section 8 constructs a stable explicit scheme for linear selfadjoint coupled wave and diffusion equations, and establishes error estimates in Theorems 5 and 6. Section 9 describes a backward reconstruction experiment in linear coupled sound and heat flow, while Section 10 deals with nonlinear coupled sound and heat flow in a non-rectangular region. Finally, some concluding remarks are offered in Section 11.

Beginning with the 1957 first edition of [4], which discussed the equations for coupled sound and heat flow, and the work in [5] dealing with hydrodynamic flow and radiation diffusion, there has been growing interest in coupled hyperbolic/parabolic systems [6–9]. Heightened interest in the semigroup properties of such coupled systems was subsequently fueled by the equations for dynamic thermoelasticity [10–21]. It is now known that several types of thermoelastic problems can be associated with holomorphic semigroups, whereas coupled sound and heat flow leads to exponentially stable semigroups that are not holomorphic. Substantial analytical interest has also developed in the time-reversed thermoelastic problem, centering on questions of backward uniqueness and continuous dependence under a-priori constraints, [22–27], [29, p. 270]. However, little seems known regarding the possibility of effective numerical computation of such backward problems. Several other examples of ill-posed inverse problems with significant applications, are discussed in [7], [28], and [29].

As is well-known [4, p. 59], for ill-posed initial value problems, all consistent time-marching difference schemes, whether explicit or implicit, are necessarily *unconditionally unstable*, and result in explosive noise amplification. The stabilized explicit schemes introduced below are unconditionally *stable*, but slightly inconsistent, and

lead to a distortion away from the true solution. This is the *stabilization penalty*. It is shown that in many problems of interest, that error is small enough to allow for useful results.

A particularly effective vehicle for computational exploration of backward in time continuation in the above systems, lies in the use of 8 bit grey scale 512×512 pixel images as initial data. As shown in Figure 1.1, many images are defined by highly non smooth intensity data. In coupled hyperbolic/parabolic systems, three distinct images are needed as initial values. In the subsequent forward evolution, these three images blend into each other, in addition to undergoing severe blurring, resulting in a solution at positive time T where these images are generally unrecognizable. Given the blurring and mixing together in the associated non-smooth intensity data at time T , recovering the original undistorted images at time $t = 0$ from the three images at time T , in the presence of numerical noise, provides a challenging test for any ill-posed reconstruction algorithm.

2. The uncertainty in backward reconstruction from imprecise data.

Consider the well-posed initial value problem

$$w_t = Aw, \quad t > 0, \quad w(x, 0) = f(x), \quad (2.1)$$

in some Banach space X with norm $\| \cdot \|_X$. Assume the system is irreversible so that the time-reversed problem is ill-posed. Backward solutions from given data at some time $T > 0$ will generally exist only for highly restricted exact solution data $w(x, T)$, satisfying certain smoothness and other requirements that are not easily characterized. Such exact data are seldom available in practice, and one must use approximate values $g(x)$ such that $\| w(\cdot, T) - g \|_X \leq \delta$, for some known small $\delta > 0$. However, the given data $g(x)$ may approximate several distinct exact solutions $w_i(x, T)$ at time T to within δ in norm, and these distinct $w_i(x, T)$ may be uniquely associated with vastly different initial data $w_i(x, 0)$, due to the discontinuous dependence on data in the time-reversed problem. Continuous dependence can be restored by restricting the class of admissible solutions based on prior knowledge, such as requiring $w(x, 0)$ to satisfy a prescribed bound, $\| w(\cdot, 0) \|_X \leq M$. It is assumed that $g(x)$ and the known constants M and δ , with $\delta \ll M$, are compatible with the existence of solutions.

This stabilized backward problem may then be stated as follows: find all solutions of $w_t = Aw$, $0 < t \leq T$, such that

$$\| w(\cdot, T) - g \|_X \leq \delta, \quad \| w(\cdot, 0) \|_X \leq M. \quad (2.2)$$

As shown in [29–35], in many cases, *logarithmic convexity* arguments can be used to prove that if $w_1(x, t)$, $w_2(x, t)$ are any two solutions of Eq. (2.2) on $[0, T]$, and if $v(x, t) = w_1(x, t) - w_2(x, t)$, then

$$\begin{aligned} \| v(\cdot, t) \|_X &\leq Const. \cdot \| v(\cdot, 0) \|_X^{1-\mu(t)} \| v(\cdot, T) \|_X^{\mu(t)}, \quad 0 \leq t \leq T, \\ &\leq Const. \cdot M^{1-\mu(t)} \delta^{\mu(t)}, \quad 0 \leq t \leq T. \end{aligned} \quad (2.3)$$

In Eq. (2.3), the Hölder exponent $\mu(t)$ satisfies $0 \leq \mu(t) \leq 1$, with $\mu(t) > 0$ for $t > 0$, $\mu(0) = 0$, $\mu(T) = 1$, and $\mu(t) \downarrow 0$ monotonically as $t \downarrow 0$. For any given fixed $t > 0$, the difference $\| v(\cdot, t) \|_X$ will be small, provided δ is sufficiently small. To the extent that Eq. (2.3) is sharp, the right hand side of that inequality represents the *fundamental uncertainty* in backward reconstruction at time $t < T$, from given noisy data $g(x)$ at time T .

When the operator A in Eq. (2.1) is an autonomous linear selfadjoint operator in a Hilbert space X , then $\mu(t) = t/T$. This is the most desirable situation. However, in other non-autonomous or nonlinear problems, the behavior in $\mu(t)$ is generally sublinear, and rapid exponential decay of $\mu(t)$ to zero as $t \downarrow 0$, may be possible. This is the case, for example, in the Navier-Stokes equations [34]. The rate at which $\mu(t) \downarrow 0$, is reflective of the rate at which the forward evolution equation $w_t = Aw$ in Eq. (2.1) has forgotten the past, and hence, of the subsequent difficulty of reconstructing the past from imperfect knowledge of the present.

As the following explicit example indicates, even a simple linear, one-dimensional evolution equation, with a non-negative smooth solution, can present quite difficult backward recovery problems. With a constant $c > 0$, consider the initial value problem

$$\begin{aligned} w_t &= e^{ct} w_{xx}, \quad 0 < x < \pi, \quad t > 0, & w_x(0) &= w_x(\pi) = 0, \\ w(x, 0) &= 1 + \cos x, \end{aligned} \tag{2.4}$$

whose exact solution is $w_{exact}(x, t) = 1 + \exp\{(1 - e^{ct})/c\} \cos x$. Let $g(x) \equiv 1$, and let $v(x, t) = \exp\{(1 - e^{ct})/c\} \cos x$, so that $w_{exact} = g + v$.

With $c = 5$, consider backward reconstruction of $w_{exact}(x, t)$ from the approximate data $g(x) \equiv 1$ at $T = 1$, given the prescribed bound $\|w_{exact}(\cdot, 0)\|_\infty \leq M = 2$. We have $\|w_{exact}(\cdot, T) - g\|_\infty = \|v(\cdot, T)\|_\infty = \delta < 1.6 \times 10^{-13}$.

The candidate reconstruction $u(x, t) \equiv 1$ is perfectly valid, and satisfies the error estimate

$$\begin{aligned} \|u(\cdot, t) - w_{exact}(\cdot, t)\|_\infty &= \|v(\cdot, t)\|_\infty = \|v(\cdot, 0)\|_\infty^{1-\mu(t)} \|v(\cdot, T)\|_\infty^{\mu(t)}, \\ &= \delta^{\mu(t)}, \end{aligned} \tag{2.5}$$

where $\mu(t) = (e^{ct} - 1)/(e^{cT} - 1) \approx e^{-c(T-t)}$. Here, despite the fact that at $t = T = 1$, we have $\delta < 1.6 \times 10^{-13}$, we find $\delta^{\mu(t)} > 0.6$ at $t = 0.25$, due to the exponential decay in $\mu(t)$. This rapid loss of accuracy as $t \downarrow 0$, eventually results in a *false* reconstruction of the smooth non negative initial values $w_{exact}(x, 0) = 1 + \cos x$, at $t = 0$.

3. A stabilized explicit scheme for the irreversible thermoelastic plate initial value problem. Let Ω be a bounded domain in R^2 with a smooth boundary $\partial\Omega$. Let $\langle \cdot, \cdot \rangle$ and $\|\cdot\|_2$, respectively denote the scalar product and norm on $\mathcal{L}^2(\Omega)$. Let L denote a linear, second order, time-independent, *positive definite* selfadjoint variable coefficient elliptic differential operator in Ω , with homogeneous Dirichlet boundary conditions on $\partial\Omega$. Let $\{\phi_m\}_{m=1}^\infty$ be the complete set of orthonormal eigenfunctions for L on Ω , and let $\{\lambda_m\}_{m=1}^\infty$, satisfying

$$0 < \lambda_1 \leq \lambda_2 \leq \dots \leq \lambda_m \leq \dots \uparrow \infty, \tag{3.1}$$

be the corresponding eigenvalues.

The following coupled hyperbolic parabolic system models a simplified thermoelastic plate problem with homogeneous *hinged* boundary conditions. This problem has been studied by several authors [11, 13–15, 18–20, 23, 24]. With L , λ_m , ϕ_m as in Eq. (3.1), and positive constants α , β , consider the linear initial value problem on

$\Omega \times (0, T]$,

$$\begin{aligned}
 u_t &= -\beta Lu - \alpha Lv, \\
 v_t &= Lw + \alpha Lu, \\
 w_t &= -Lv, \\
 u(x, y, 0) &= f(x, y), \quad v(x, y, 0) = g(x, y), \quad w(x, y, 0) = h(x, y), \\
 u(x, y, t) &= v(x, y, t) = w(x, y, t) = 0, \quad (x, y, t) \in \partial\Omega \times [0, T].
 \end{aligned} \tag{3.2}$$

With $L = -\Delta$, $w = \Delta z$, $v = z_t$, the above system corresponds to the thermoelastic plate problem $z_{tt} = -\Delta^2 z - \alpha \Delta u$, $u_t = \beta \Delta u + \alpha \Delta z_t$, with $u = z = \Delta z = 0$ on $\partial\Omega$.

The initial value problem Eq. (3.2) becomes ill-posed when the time direction is reversed. We contemplate such time-reversed computations by allowing for possible *negative* time steps Δt in the explicit difference scheme Eq.(3.8) below. With λ_m as in Eq. (3.1), the positive constants α , β and the operator L as in Eq. (3.2), fix $\omega > 0$ and $p > 1$. Given Δt , define ν , Λ , Q , ζ_m , r_m , as follows:

$$\begin{aligned}
 \nu &= (3 + \alpha + \alpha^2 + 2\beta), \quad \Lambda = \nu(I + L), \quad Q = \exp(-\omega|\Delta t|\Lambda^p), \\
 \zeta_m &= \nu(1 + \lambda_m) > 3, \quad r_m = \exp(-\omega|\Delta t|(\zeta_m)^p), \quad m \geq 1.
 \end{aligned} \tag{3.3}$$

For the purpose of the present theoretical development of stabilizing smoothing operators such as Q , the family $\{\lambda_m, \phi_m\}$ in Eq. (3.1), is assumed *known or precomputed*. However, as will be illustrated in Sections 7 and 10 below, in many practical computations, a different smoothing operator, based on a substitute elliptic operator L^\dagger with known characteristic pairs, such as the negative Laplacian, can be used instead. Since $p > 1$ has non integer values typically, both the operators Λ^p and Q in Eq. (3.3), must be synthesized in terms of the characteristic pairs $\{\lambda_m, \phi_m\}$ of L . With ζ_m , r_m as in Eq. (3.3), define for every $h \in \mathcal{L}^2(\Omega)$,

$$\Lambda^p h = \sum_{m=1}^{\infty} (\zeta_m)^p \langle h, \phi_m \rangle \phi_m, \quad Qh = \sum_{m=1}^{\infty} r_m \langle h, \phi_m \rangle \phi_m. \tag{3.4}$$

Let G , S , and P , be the following 3×3 matrices

$$G = \begin{bmatrix} -\beta L & -\alpha L & 0 \\ \alpha L & 0 & L \\ 0 & -L & 0 \end{bmatrix}, \quad S = \begin{bmatrix} Q & 0 & 0 \\ 0 & Q & 0 \\ 0 & 0 & Q \end{bmatrix}, \quad P = \begin{bmatrix} \Lambda^p & 0 & 0 \\ 0 & \Lambda^p & 0 \\ 0 & 0 & \Lambda^p \end{bmatrix}. \tag{3.5}$$

Let W be the three component vector $[u, v, w]^T$. We may rewrite Eq. (3.2) as the equivalent first order system,

$$W_t = GW, \quad 0 < t \leq T_{max}, \quad W(\cdot, 0) = [f, g, h]^T. \tag{3.6}$$

We shall study an explicit time-marching finite difference scheme for Eq.(3.6), in which only the time variable is discretized, while the space variables remain continuous. With a given positive integer N , let $|\Delta t| = T_{max}/N$ be the time step magnitude, and let W^n denote $W(\cdot, n\Delta t)$, $n = 0, 1, \dots, N$. If $W(\cdot, t)$ is the unique solution of Eq.(3.6), then

$$W^{n+1} = W^n + \Delta t GW^n + \tau^n, \tag{3.7}$$

where the ‘truncation error’ $\tau^n = \frac{1}{2}(\Delta t)^2 G^2 W(\tilde{t})$, with $n|\Delta t| < \tilde{t} < (n+1)|\Delta t|$. With G and S as in Eq.(3.5), let R be the linear operator $R = S + \Delta t SG$. Using the smoothing operator S , we consider approximating W^n with $U^n \equiv [u^n, v^n, w^n]^T$, where

$$U^{n+1} = SU^n + \Delta t SGU^n \equiv RU^n, \quad n = 0, 1, \dots, (N-1), \quad U^0 = [f, g, h]^T. \quad (3.8)$$

With $\Delta t > 0$ and the data U^0 at time $t = 0$, the forward marching scheme in Eq.(3.8) aims to solve a well-posed problem. However, with $\Delta t < 0$, together with *appropriate* data U^0 at time T_{max} , marching backward from T_{max} in Eq.(3.8) attempts to solve an ill-posed problem. It remains to be seen whether U^n can be a useful approximation to W^n , by proper choices of ω , p , and $|\Delta t|$. Define the following norms for three component vectors such as $W(\cdot, t)$ and U^n ,

$$\begin{aligned} \|W(\cdot, t)\|_2 &= \left\{ \|u(\cdot, t)\|_2^2 + \|v(\cdot, t)\|_2^2 + \|w(\cdot, t)\|_2^2 \right\}^{1/2}, \\ \|U^n\|_2 &= \left\{ \|u^n\|_2^2 + \|v^n\|_2^2 + \|w^n\|_2^2 \right\}^{1/2}, \\ \|W\|_{2,\infty} &= \sup_{0 \leq t \leq T_{max}} \{ \|W(\cdot, t)\|_2 \}. \end{aligned} \quad (3.9)$$

LEMMA 1. *With $p > 1$, and ζ_m, r_m , as in Eq.(3.3), fix a positive integer J , and choose $\omega \geq (\zeta_J)^{1-p}$. Then,*

$$r_m(1 + |\Delta t|\zeta_m) \leq 1 + |\Delta t|\zeta_J, \quad m \geq 1. \quad (3.10)$$

Proof: The inequality in Eq. (3.10) is valid for $1 \leq m \leq J$, in view of Eq. (3.1). For $m > J$,

$$\exp\{-\omega|\Delta t|(\zeta_m)^p\} \leq \exp\{-\omega|\Delta t|\zeta_m(\zeta_J)^{p-1}\} \leq \exp\{-|\Delta t|\zeta_m\}, \quad (3.11)$$

since $\omega(\zeta_J)^{p-1} \geq 1$. Also, $\exp\{-|\Delta t|\zeta_m\} \leq (1 + |\Delta t|\zeta_m)^{-1}$, since $1 + x \leq e^x$ for real x . Hence, for $m > J$, $r_m(1 + |\Delta t|\zeta_m) \leq 1$. QED.

LEMMA 2. *With ω, p, ζ_J , as in Lemma 1, and R as in Eq.(3.8), we have $\|R\|_2 \leq 1 + |\Delta t|\zeta_J$. The explicit scheme in Eq.(3.8) is unconditionally stable, and*

$$\|U^n\|_2 = \|R^n U^0\|_2 \leq \exp\{n|\Delta t|\zeta_J\} \|U^0\|_2, \quad n = 1, 2, \dots, N. \quad (3.12)$$

Proof: In the system $U^{n+1} = SU^n + \Delta t SGU^n$, expand in the orthonormal eigenfunctions ϕ_m , using $L\phi_m = \lambda_m\phi_m$. Let $u^n = \sum_{m=1}^{\infty} u_m^n \phi_m$, $v^n = \sum_{m=1}^{\infty} v_m^n \phi_m$, $w^n = \sum_{m=1}^{\infty} w_m^n \phi_m$, where $g_m^n = \langle g^n, \phi_m \rangle$. Then, with r_m as in Eq.(3.3),

$$\begin{aligned} u_m^{n+1} &= r_m u_m^n - r_m \lambda_m \Delta t (\beta u_m^n + \alpha v_m^n), \\ v_m^{n+1} &= r_m v_m^n + r_m \lambda_m \Delta t (\alpha u_m^n + w_m^n), \\ w_m^{n+1} &= r_m w_m^n - r_m \lambda_m \Delta t v_m^n. \end{aligned} \quad (3.13)$$

Hence,

$$\begin{aligned}
 |u_m^{n+1}|^2 &\leq r_m^2 |u_m^n|^2 + r_m^2 \Delta t^2 |\beta \lambda_m u_m^n + \alpha \lambda_m v_m^n|^2 + 2r_m^2 |\Delta t| |u_m^n| |\beta \lambda_m u_m^n + \alpha \lambda_m v_m^n|, \\
 |v_m^{n+1}|^2 &\leq r_m^2 |v_m^n|^2 + r_m^2 \lambda_m^2 \Delta t^2 |\alpha u_m^n + w_m^n|^2 + 2r_m^2 \lambda_m |\Delta t| |v_m^n| |\alpha u_m^n + w_m^n|, \\
 |w_m^{n+1}|^2 &\leq r_m^2 |w_m^n|^2 + r_m^2 \lambda_m^2 \Delta t^2 |v_m^n|^2 + 2r_m^2 \lambda_m |\Delta t| |w_m^n v_m^n|.
 \end{aligned} \tag{3.14}$$

Next, using $2xy \leq x^2 + y^2$,

$$\begin{aligned}
 2r_m^2 |\Delta t| |u_m^n| |\beta \lambda_m u_m^n + \alpha \lambda_m v_m^n| &\leq 2r_m^2 |\Delta t| \beta \lambda_m |u_m^n|^2 + 2r_m^2 |\Delta t| \alpha \lambda_m |u_m^n v_m^n|, \\
 &\leq r_m^2 |\Delta t| (2\beta + \alpha) \lambda_m |u_m^n|^2 + r_m^2 |\Delta t| \alpha \lambda_m |v_m^n|^2,
 \end{aligned} \tag{3.15}$$

and

$$r_m^2 \Delta t^2 |\beta \lambda_m u_m^n + \alpha \lambda_m v_m^n|^2 \leq 2r_m^2 \Delta t^2 \beta^2 \lambda_m^2 |u_m^n|^2 + 2r_m^2 \Delta t^2 \alpha^2 \lambda_m^2 |v_m^n|^2. \tag{3.16}$$

Likewise,

$$2r_m^2 \lambda_m |\Delta t| |v_m^n| |\alpha u_m^n + w_m^n| \leq r_m^2 |\Delta t| \lambda_m \{2|v_m^n|^2 + \alpha^2 |u_m^n|^2 + |w_m^n|^2\}, \tag{3.17}$$

and

$$r_m^2 \Delta t^2 \lambda_m^2 |\alpha u_m^n + w_m^n|^2 \leq 2r_m^2 \Delta t^2 \lambda_m^2 \{\alpha^2 |u_m^n|^2 + |w_m^n|^2\}. \tag{3.18}$$

Therefore, with $\nu = (3 + \alpha + \alpha^2 + 2\beta)$, $\zeta_m = \nu(1 + \lambda_m)$,

$$\begin{aligned}
 &|u_m^{n+1}|^2 + |v_m^{n+1}|^2 + |w_m^{n+1}|^2 \leq \\
 &|u_m^n|^2 r_m^2 \{1 + (\alpha + \alpha^2 + 2\beta) \lambda_m |\Delta t| + (2\alpha^2 + 2\beta^2) \lambda_m^2 \Delta t^2\} \\
 &+ |v_m^n|^2 r_m^2 \{1 + (3 + \alpha) \lambda_m |\Delta t| + (1 + 2\alpha^2) \lambda_m^2 \Delta t^2\} \\
 &+ |w_m^n|^2 r_m^2 \{1 + 2\lambda_m |\Delta t| + 2\lambda_m^2 \Delta t^2\} \\
 &\leq r_m^2 (1 + \zeta_m |\Delta t|)^2 (|u_m^n|^2 + |v_m^n|^2 + |w_m^n|^2),
 \end{aligned} \tag{3.19}$$

which implies Eq. (3.12) on using Lemma 1. QED

If $W(t)$ is the unique solution of Eq.(3.6) on $0 \leq t \leq T_{max}$, we get from Eq.(3.7) with $0 \leq n \leq N - 1$,

$$W^{n+1} = RW^n + (W^n - SW^n) + \Delta t(GW^n - SGW^n) + \tau^n. \tag{3.20}$$

LEMMA 3. *Let $W(t)$ be the unique solution of Eq.(3.6). Then, with S and P as in Eq.(3.5), the definitions of the norms in Eq.(3.9), and $0 \leq n \leq N$,*

$$\begin{aligned}
 \|\tau^n\|_2 &\leq 1/2(\Delta t)^2 \|G^2W\|_{2,\infty}, \\
 \|W^n - SW^n\|_2 &\leq \omega |\Delta t| \|PW\|_{2,\infty}, \\
 |\Delta t| \|GW^n - SGW^n\|_2 &\leq \omega (\Delta t)^2 \|PGW\|_{2,\infty}.
 \end{aligned} \tag{3.21}$$

Proof: The inequality for the truncation error τ^n in Eq. (3.21) follows naturally from

the definitions in Eq. (3.9). Expanding in the orthonormal eigenfunctions ϕ_m of L , and using the inequality $1 - e^{-x} \leq x$ for all real x , we get

$$\begin{aligned} \|W^n - SW^n\|_2^2 &= \sum_{m=0}^{\infty} (1 - r_m)^2 (|u_m^n|^2 + |v_m^n|^2 + |w_m^n|^2), \\ &\leq \sum_{m=0}^{\infty} (\omega|\Delta t|(\zeta_m)^p)^2 (|u_m^n|^2 + |v_m^n|^2 + |w_m^n|^2), \\ &= (\omega\Delta t)^2 (\|PW^n\|_2^2). \end{aligned} \quad (3.22)$$

This proves the second inequality in Eq. (3.21). The last inequality is a corollary of the second. QED.

4. The stabilization penalties in the forward and backward problems.

Explicit time differencing in systems of partial differential involving heat conduction, generally requires stringent Courant stability restrictions on the time step Δt . The stabilizing smoothing operator S in the explicit scheme in Eq.(3.8) leads to unconditional stability, but at the cost of introducing a small error at each time step. We must now assess the cumulative effect of that error. If the accumulated error at the final time T_{max} is sufficiently small, the stabilized explicit scheme would offer considerable advantages in the computation of multidimensional problems on fine meshes.

We have the following result for the stabilization penalty in the well-posed forward problem.

THEOREM 1. *With $\Delta t > 0$, let W^n be the unique solution of Eq.(3.6) at $t = n\Delta t$. Let U^n be the corresponding solution of the forward explicit scheme in Eq. (3.8), and let p, ζ_J, ω , be as in Lemma 1. If $ER(t) \equiv U^n - W^n$, denotes the error at $t = n\Delta t$, $n = 0, 1, 2, \dots, N$, we have*

$$\begin{aligned} \|ER(t)\|_2 &\leq e^{t\zeta_J} \|ER(0)\|_2 + \{\omega(e^{t\zeta_J} - 1)/\zeta_J\} \|PW\|_{2,\infty} \\ &+ \{(e^{t\zeta_J} - 1)/\zeta_J\} \{\omega\Delta t \|PGW\|_{2,\infty} + (\Delta t/2) \|G^2W\|_{2,\infty}\}. \end{aligned} \quad (4.1)$$

Proof: Let $H^n = \tau^n + (W^n - SW^n) + \Delta t(GW^n - SGW^n)$. Then, $W^{n+1} = RW^n + H^n$, while $U^{n+1} = RU^n$. Therefore

$$U^{n+1} - W^{n+1} = R(U^n - W^n) + H^n = R^{n+1}ER(0) + \Delta t \sum_{j=0}^n R^{n-j} H^j / (\Delta t). \quad (4.2)$$

Hence, using Lemma 2, and letting $t = (n+1)\Delta t$,

$$\begin{aligned} \|ER(t)\|_2 &\leq e^{t\zeta_J} \|ER(0)\|_2 + \{\|H\|_{2,\infty}/\Delta t\} \Delta t \sum_{j=0}^n \|R^{n-j}\|_2, \\ &\leq e^{t\zeta_J} \|ER(0)\|_2 + \{\|H\|_{2,\infty}/\Delta t\} \int_0^t e^{\zeta_J(t-u)} du \\ &= e^{t\zeta_J} \|ER(0)\|_2 + \{\|H\|_{2,\infty}/\Delta t\} (e^{t\zeta_J} - 1)/\mu_J. \end{aligned} \quad (4.3)$$

Next, using Lemma 3 to estimate $\{\|H\|_{2,\infty}/\Delta t\}$, one obtains Eq. (4.1) from Eq. (4.3). QED.

In the forward problem, we may assume the given data $U^0 = [f, g, h]^T$ to be known with sufficiently high accuracy that one may set $ER(0) = 0$ in Eq.(4.1). Choosing $\omega = (\zeta_J)^{1-p}$ in Lemma 1, Eq.(4.1) reduces to

$$\| ER(t) \|_2 \leq (\zeta_J)^{-p} (e^{t\zeta_J} - 1) \| PW \|_{2,\infty} + O(\Delta t), \quad 0 \leq t \leq T_{max}. \quad (4.4)$$

Therefore, when using the explicit scheme in Eq.(3.8), there remains the non-vanishing residual error $(\zeta_J)^{-p} (e^{t\zeta_J} - 1) \| PW \|_{2,\infty}$, as $\Delta t \downarrow 0$. This is the *stabilization penalty*, which results from smoothing at each time step, and grows monotonically as $t \uparrow T_{max}$. Clearly, if T_{max} is large, the accumulated distortion may become unacceptably large as $t \uparrow T_{max}$, and the stabilized explicit scheme is not useful in that case. On the other hand, if T_{max} is small, as is the case in problems involving small values of t , it may be possible to choose $p > 2$ and large ζ_J , yet with small enough $\zeta_J T_{max}$ that $(\zeta_J)^{-p} (e^{\zeta_J T_{max}} - 1)$ is quite small. In that case, the stabilization penalty remains acceptable on $0 \leq t \leq T_{max}$. As an example, with $T_{max} = 10^{-3}$, $p = 2.75$, and $\zeta_J = 10^4$, we find $(\zeta_J)^{-p} (e^{\zeta_J T_{max}} - 1) < 2.21 \times 10^{-7}$. For this important but limited class of problems, the absence of restrictive Courant conditions on the time step Δt in the explicit scheme in Eq.(3.8), provides a significant advantage in well-posed forward computations of multidimensional problems on fine meshes.

There is an additional penalty in the ill-posed backward problem. As noted in Section 2, in marching backward from $t = T_{max}$, solutions exist only for a restricted class of data satisfying certain smoothness constraints. Such data are seldom known with sufficiently high accuracy. We shall assume that the given data $U_b = [f_b, g_b, h_b]^T$ at $t = T_{max}$, differs from such unknown exact data $W(\cdot, T_{max})$ by small amounts:

$$\| U_b - W(\cdot, T_{max}) \|_2 \leq \delta. \quad (4.5)$$

This leads to the following result.

THEOREM 2. *With $\Delta t < 0$, let W^n be the unique solution of the forward well-posed problem in Eq.(3.6) at $s = T_{max} - n|\Delta t|$. Let U^n be the solution of the backward explicit scheme in Eq. (3.8), with initial data $U(0) = U_b = [f_b, g_b, h_b]^T$ as in Eq.(4.5). Let p, ζ_J, ω , be as in Lemma 1. If $ER(s) \equiv U^n - W^n$, denotes the error at $s = T_{max} - n|\Delta t|$, $n = 0, 1, 2, \dots, N$, we have, with δ as in Eq.(4.5),*

$$\begin{aligned} \| ER(s) \|_2 \leq & \delta e^{n|\Delta t|\zeta_J} + \left\{ \omega (e^{n|\Delta t|\zeta_J} - 1) / \zeta_J \right\} \| PW \|_{2,\infty} \\ & + \left\{ (e^{n|\Delta t|\zeta_J} - 1) / \zeta_J \right\} \left\{ \omega |\Delta t| \| PGW \|_{2,\infty} + (|\Delta t|/2) \| G^2 W \|_{2,\infty} \right\}. \end{aligned} \quad (4.6)$$

Proof: Let $H^n = \tau^n + (W^n - SW^n) + \Delta t(GW^n - SGW^n)$. Then, $W^{n+1} = RW^n + H^n$, while $U^{n+1} = RU^n$. Therefore

$$U^{n+1} - W^{n+1} = R(U^n - W^n) + H^n = R^{n+1}ER(0) + |\Delta t| \sum_{j=0}^n R^{n-j} H^j / (|\Delta t|). \quad (4.7)$$

Hence, using Lemma 2, and with $t = (n+1)|\Delta t|$,

$$\begin{aligned} \| U^{n+1} - W^{n+1} \|_2 \leq & \delta e^{t\zeta_J} + \{ \| H \|_{2,\infty} / |\Delta t| \} |\Delta t| \sum_{j=0}^n \| R^{n-j} \|_2, \\ \leq & \delta e^{t\zeta_J} + \{ \| H \|_{2,\infty} / |\Delta t| \} \int_0^t e^{\zeta_J(t-u)} du. \end{aligned} \quad (4.8)$$

As in the preceding Theorem, we may now use Lemma 3 to estimate $\{|||H|||_{2,\infty}/|\Delta t|\}$ and obtain Eq.(4.6) from Eq.(4.8). QED.

It is instructive to compare the results in the well-posed case in Eq.(4.4), with the ill-posed results implied by Eq.(4.6). For this purpose, we must reevaluate Eq.(4.6) at the same t values that are used in Eq.(4.4). With $\Delta t > 0$, $t = k\Delta t$, and $W^k = W(k\Delta t)$, let U^k now denote the precomputed backward solution evaluated at $t = k\Delta t$. Let $ER(t) = U^k - W^k$, $k = 0, 1, 2, \dots, N$, with $T_{max} = N\Delta t$. Again, choosing $\omega = (\zeta_J)^{1-p}$, we get from Eq.(4.6),

$$\begin{aligned} \| ER(t) \|_2 \leq & (\zeta_J)^{-p} \{ \exp[\zeta_J(T_{max} - t)] - 1 \} |||PW|||_{2,\infty} \\ & + \delta \exp\{\zeta_J(T_{max} - t)\} + O(\Delta t), \quad 0 \leq t \leq T_{max}. \end{aligned} \quad (4.9)$$

Here, the stabilization penalty is augmented by an additional term, resulting from amplification of the error δ in the given data at $t = T_{max}$, as shown in Eq.(4.5). Both of these terms grow monotonically as $t \downarrow 0$, reflecting backward in time marching from $t = T_{max}$.

Again, with large T_{max} , the non-vanishing residuals in Eq. (4.9) as $|\Delta t| \downarrow 0$, lead to large errors, and the backward explicit scheme is not useful in such cases. However, there is an important class of ill-posed backward problems, problems with small T_{max} and small δ , for which Eq.(4.9) leads to *almost optimal* results. In addition to Eq.(4.5), assume $W(x, 0)$ satisfies a prescribed \mathcal{L}^2 bound M . These a-priori constraints are expressed as follows

$$\| W(\cdot, T_{max}) - U_b \|_2 \leq \delta, \quad \| W(\cdot, 0) \|_2 \leq M. \quad (4.10)$$

We now choose ζ_J in terms of M and δ , and define $\beta(t)$ as follows

$$\zeta_J = (1/T_{max}) \log(M/\delta), \quad \beta(t) = t/T_{max}. \quad (4.11)$$

With these definitions, Eq. (4.9) now becomes

$$\begin{aligned} \| ER(t) \|_2 \leq & (\zeta_J)^{-p} \{ \exp[\zeta_J(T_{max} - t)] - 1 \} |||PW|||_{2,\infty} \\ & + M^{1-\beta(t)} \delta^{\beta(t)} + O(\Delta t), \quad 0 \leq t \leq T_{max}. \end{aligned} \quad (4.12)$$

The second term on the right in Eq. (4.12) represents the fundamental uncertainty in ill-posed backward continuation from noisy data, for solutions satisfying prescribed bounds, as in Eq. (4.10). As noted in Section 2, with $\beta(t) = t/T_{max}$, the uncertainty $M^{1-\beta(t)} \delta^{\beta(t)}$ is known to be *best-possible* in the case of autonomous selfadjoint problems, [31], [32]. The first term in Eq. (4.12), which is also present in the forward problem, is the penalty that must be incurred for computing multidimensional problems, using simple explicit schemes without stringent Courant restrictions on the time step Δt . In many problems of interest, the choice of ζ_J in Eq. (4.11), together with a suitable value of $p > 2$, can make that first term small enough to enable useful backward recovery in Eq.(3.6). For example, with parameter values such as $T_{max} = 10^{-3}$, $M = 10^2$, $\delta = 10^{-3}$, $p = 2.75$, we have $M/\delta = 10^5 = \exp\{\zeta_J T_{max}\}$, and $(\zeta_J)^{-p} < 6.79 \times 10^{-12}$. We would then obtain from Eq. (4.12),

$$\begin{aligned} \| ER(t) \|_2 \leq & M^{1-\beta(t)} \delta^{\beta(t)} \\ & + (6.79 \times 10^{-7}) |||PW|||_{2,\infty} + O(\Delta t), \quad 0 \leq t \leq T_{max}. \end{aligned} \quad (4.13)$$

Remark 1. The above analysis, valid in general domains $\Omega \in R^2$, assumes knowledge of the complete set of characteristic pairs $\{\lambda_m, \phi_m\}$ of the elliptic operator L , to enable synthesis of the smoothing operator Q in Eq. (3.3). As discussed in Section 6 below, and illustrated in Section 7, in several special domains, an equivalent smoothing operator Q^\dagger may readily be available on that particular domain, and one may dispense with complete knowledge of $\{\lambda_m, \phi_m\}$.

However, in other cases, precomputing a sufficiently large number K of eigenpairs $\{\lambda_m, \phi_m\}$ of a linear selfadjoint elliptic operator L on a general domain Ω , may well be warranted. If the operator L is representative of a class of more general, possibly nonlinear, differential operators \tilde{L} , one may be able to synthesize a useful smoothing operator Q using the first K eigenpairs of L , and use it to stabilize explicit schemes for several time-reversed nonlinear equations. Computational methods for elliptic eigenvalue problems are discussed in [36–38].

Remark 2. In most practical applications of ill-posed backward problems, the values of M and δ in Eq. (4.10) are seldom known accurately. In many cases, interactive adjustment of the parameter pair (ω, p) in the definition of Q in Eq. (3.3), based on prior knowledge about the exact solution, is crucial in obtaining useful reconstructions. This process is similar to the manual tuning of an FM station, or the manual focusing of binoculars, and likewise requires user recognition of a ‘correct’ solution.

5. Linear computational experiment on backward in time reconstruction in thermoelastic plate. With Ω the open unit square $0 < x, y < 2\pi$, and $0 \leq t \leq T_{max} = 7.5 \times 10^{-3}$, we consider the following thermoelastic plate problem on $\Omega \times (0, T_{max})$, $z_{tt} = -\Delta^2 z - \alpha \Delta u$, $u_t = \beta \Delta u + \alpha \Delta z_t$. Here, $u(x, y, t)$ denotes the temperature, $z(x, y, t)$ the displacement, $z_t(x, y, t)$ the velocity, $\alpha = 1$, $\beta = 2$, and $u = z = \Delta z = 0$ on $\partial\Omega \times [0, T_{max}]$. See [11, 14, 15, 18].

Putting $v = z_t$, $w = \Delta z$, and now referring to $w(x, y, t)$ as the ‘displacement’, we obtain the equivalent first order system

$$\begin{aligned} u_t &= \beta \Delta u + \alpha \Delta v, \\ v_t &= -\Delta w - \alpha \Delta u, \\ w_t &= \Delta v, \\ u(x, y, 0) &= f(x, y), \quad v(x, y, 0) = g(x, y), \quad w(x, y, 0) = h(x, y), \\ u(x, y, t) &= v(x, y, t) = w(x, y, t) = 0, \quad (x, y, t) \in \partial\Omega \times [0, T_{max}]. \end{aligned} \tag{5.1}$$

In this computational experiment, the initial values $f(x, y)$, $h(x, y)$, $g(x, y)$, are the intensity data that define the three images shown in the top row of Figure 5.1. These are 8 bit grey scale 512×512 images with intensity values ranging from 0 to 255. We may interpret the MRI brain image $f(x, y)$, as representing temperature above (or below) a reference level, measured in tenths of a degree. Likewise, the USAF resolution chart image $h(x, y)$, may represent deflection from equilibrium, measured in tenths of a millimeter, while the satellite image $g(x, y)$ may represent velocity in appropriate units.

All three initial values are non-negative functions on Ω . However, at positive values of t , $u(x, y, t)$, $v(x, y, t)$, $w(x, y, t)$, may develop substantial negative values as a natural consequence of the evolution in Eq. (5.1). Accurate knowledge of these negative values is essential for successful backward recovery. We write

$$\begin{aligned} u^+(x, y, t) &= \max\{u(x, y, t), 0\} \geq 0, \quad u^-(x, y, t) = -\min\{u(x, y, t), 0\} \geq 0, \\ u(x, y, t) &= u^+(x, y, t) - u^-(x, y, t), \end{aligned} \tag{5.2}$$

with a similar decomposition for $v(x, y, t)$ and $w(x, y, t)$.

With $\Delta x = \Delta y = (2\pi)/512$, a uniform spatial grid was placed on Ω . Taking advantage of the constant coefficient differential operators in Eq. (5.1), highly accurate Fourier methods for spatial discretization can be used, based on FFT algorithms. Using $\Delta t = 3 \times 10^{-7}$, and choosing $T_{max} = 25000\Delta t = 7.5 \times 10^{-3}$, stable forward numerical computation was carried out on $[0, T_{max}]$. The resulting values of $u^+(x, y, T_{max})$, $v^+(x, y, T_{max})$, $w^+(x, y, T_{max})$, are displayed as the three images in the middle row of Figure 5.1.

Evidently, each of the three images in the middle row has been corrupted by the other two images, while undergoing severe blurring. The computed data $u(x, y, T_{max})$, $v(x, y, T_{max})$, $w(x, y, T_{max})$, while unavoidably affected by discretization errors and numerical noise, are presumed to be a good approximation to the true solution of Eq. (5.1) at $t = T_{max}$.

Using these data, and the previous values of Δx , Δy , and Δt , the stabilized explicit scheme in Eq. (3.8) was run backward 25000 time steps from T_{max} . Here, the fact that Ω is a rectangular region with L the negative Laplacian, is a significant advantage. The characteristic pairs of L are known explicitly, and FFT algorithms can be used to synthesize the smoothing operator Q in Eq. (3.3). As discussed in Remark 2 above, interactive adjustment of the parameter pair (ω, p) in the definition of Q , based on prior knowledge about the solution, was found helpful. The pair $\omega = 3.0 \times 10^{-8}$, $p = 3.275$, produced the reconstruction shown in the bottom row of Figure 5.1. Here, $u^+(x, y, 0)$, $v^+(x, y, 0)$, $w^+(x, y, 0)$, were chosen as the reconstructed solution, based on prior knowledge that the correct initial values are non-negative functions on Ω . Additional information on this reconstruction is provided in Figures 5.2. Magnification of the images in these two Figures is helpful.

Clearly, substantial reconstruction has been achieved from severely blurred data. Since the operator L in this experiment is linear, autonomous, and selfadjoint, the error estimate in Eq. (4.12) in Section 5.2 applies. With $T_{max} = 7.5 \times 10^{-3}$, $\omega = 3.0 \times 10^{-8}$, $p = 3.275$, we obtain from $\omega = (\zeta_J)^{(1-p)}$, that $\zeta_J = 2027$ and $\zeta_J T_{max} = 15.2$. Hence, $(\zeta_J)^{-p} \{\exp(\zeta_J T_{max}) - 1\} < 5.91 \times 10^{-5}$, which indicates a small value for the first term on the right of Eq. (4.12). This ‘stabilization penalty’ is the price paid for avoiding the explosive computational instability that results when using stepwise marching schemes in ill-posed initial value problems, [4, p. 59].

Figure 5.2 draws attention to the distortion and subsequent recovery of the actual intensity data that define the MRI brain image. As the plots for $u^+(x, y, T_{max})$, $u^-(x, y, T_{max})$ indicate, the input data at time T_{max} develop significant negative values, while displaying substantial transformation from the original data at time $t = 0$. The plots for the recovered data at time $t = 0$ are not identical to the original plots at $t = 0$. Such discrepancies are anticipated by the presence of the second term on the right in Eq. (4.12). As discussed in Section 2, there is a necessary uncertainty in reconstructing the past from imperfect knowledge of the present.

BACKWARD RECOVERY IN LINEAR THERMOELASTIC PLATE PROBLEM WITH CONSTANT COEFFICIENTS.

Using input data at positive time T , shown in middle row, explicit scheme marching backward in time seeks to recover true initial data at time 0, shown in top row. Actually recovered data are shown in last row.

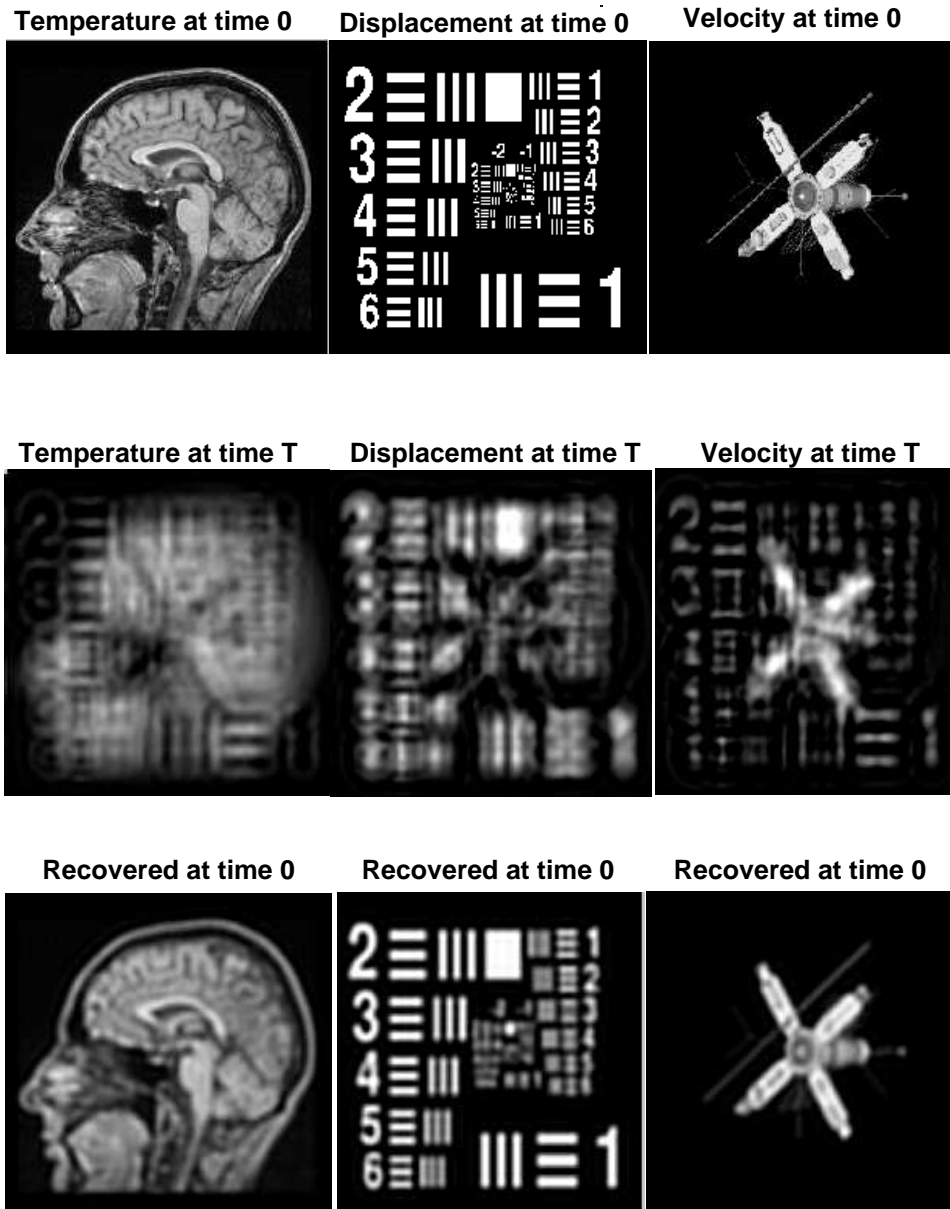


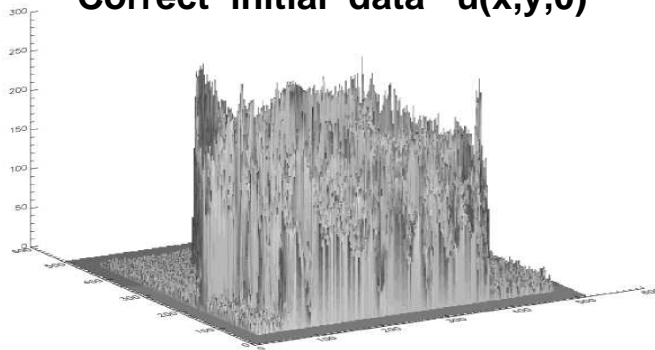
FIG. 5.1. Linear thermoelastic experiment in Section 5 shows severe distortion and blurring of initial data in forward evolution up to time T_{max} , followed by successful backward in time reconstruction using stabilized explicit scheme in Eq. (3.8).

BACKWARD RECOVERY OF INITIAL TEMPERATURE DATA IN LINEAR CONSTANT COEFFICIENT PROBLEM. INPUT DATA AT POSITIVE TIME T HAVE SIGNIFICANT NEGATIVE VALUES.

Temperature at time 0



Correct initial data $u(x,y,0)$

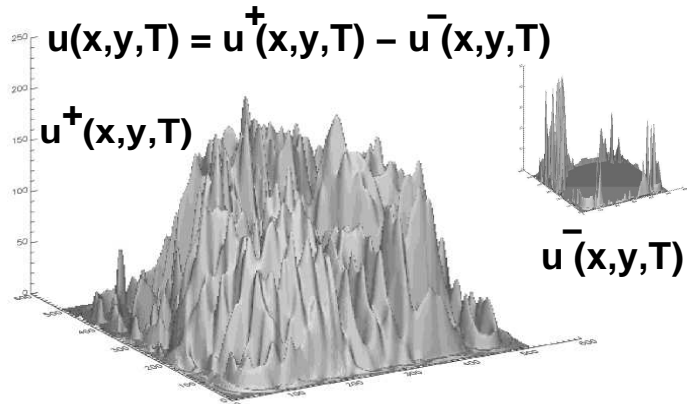


Temperature at time T

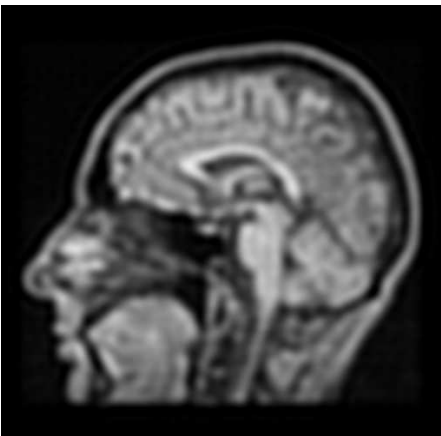


Input data $u(x,y,T)$ at positive time T

$$u(x,y,T) = u^+(x,y,T) - u^-(x,y,T)$$



Recovered at time 0



Recovered data $u(x,y,0)$

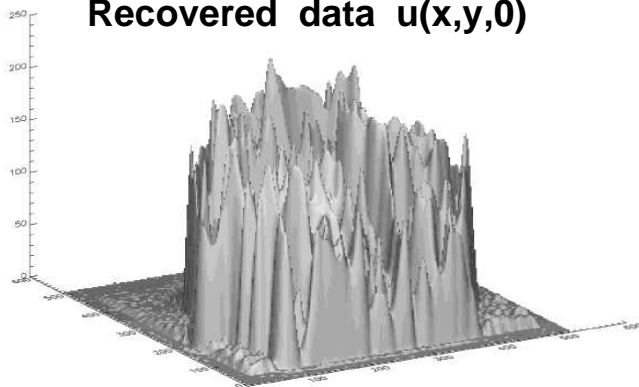


FIG. 5.2. Severe distortion along with development of negative values in forward evolution of temperature data up to time T_{max} , in linear thermoelastic experiment in Section 5. As discussed in Section 2, inexact input data at time T_{max} results in small discrepancies in backward recovery at $t = 0$.

6. Substitute smoothing operators. Using the Laplacian for smoothing when L has variable coefficients. As noted in Remark 1, the developments in Sections [3-5] presuppose knowledge of the characteristic pairs of the variable coefficient elliptic operator L , or the precomputation of a sufficiently large number of such pairs. However, it is often possible to use a substitute smoothing operator Q^\dagger , based on a different elliptic operator with known characteristic pairs.

Let Δ denote the Laplacian operator in Ω , with homogeneous Dirichlet boundary conditions on $\partial\Omega$. With ν , L , Λ , as in Eq. (3.3), let $\Gamma = \nu(I - \Delta)$. For any real $q > 1$ and $\epsilon > 0$, define

$$Q_\Delta = \exp\{-\epsilon|\Delta t| \Gamma^q\}, \quad (6.1)$$

Closed form expressions for the eigenfunctions of the Laplacian are known for specific domains that are important in applications, including rectangles, circles, and spheres [39]. On such domains, it may be advantageous to construct smoothing operators Q_Δ based on the Laplacian, in lieu of the smoothing operator Q in Eq.(3.3). Such a program is feasible for those differential operators L for which the following result is *valid*: Given any $\omega > 0$, and $p > 1$, there exist $\epsilon > 0$, and real $q \geq p$, such that for all $g \in \mathcal{L}^2(\Omega)$ and sufficiently small $|\Delta t|$,

$$\| \exp\{-\epsilon|\Delta t| \Gamma^q\}g \|_2 \leq \| \exp\{-\omega|\Delta t| \Lambda^p\}g \|_2, \implies \| Q_\Delta g \|_2 \leq \| Qg \|_2. \quad (6.2)$$

The linear operator $H = (\exp\{-\epsilon|\Delta t| \Gamma^q\})(\exp\{\omega|\Delta t| \Lambda^p\})$ is well-defined on the range of $(\exp\{-\omega|\Delta t| \Lambda^p\})$, which is dense in $\mathcal{L}^2(\Omega)$. The inequality in Eq.(6.2) would follow if it can be shown that H can be extended to a bounded operator on all of $\mathcal{L}^2(\Omega)$, with $\| H \|_2 \leq 1$.

Eq. (6.2) appears to be validated in numerous computational experiments. Results of a somewhat similar nature are known in the theory of Gaussian estimates for heat kernels. See e.g. [40–43], and the references therein.

Let S_Δ and P_Δ be the following 3×3 matrices

$$S_\Delta = \begin{bmatrix} Q_\Delta & 0 & 0 \\ 0 & Q_\Delta & 0 \\ 0 & 0 & Q_\Delta \end{bmatrix}, \quad P_\Delta = \begin{bmatrix} \Gamma^q & 0 & 0 \\ 0 & \Gamma^q & 0 \\ 0 & 0 & \Gamma^q \end{bmatrix}. \quad (6.3)$$

The Laplacian stabilized explicit scheme corresponding to Eq.(3.8) is given by

$$U^{n+1} = S_\Delta U^n + \Delta t S_\Delta G U^n \equiv R_\Delta U^n, \quad n = 0, 1, \dots, (N-1), \quad U^0 = [f, g, h]^T, \quad (6.4)$$

to which the following result applies.

LEMMA 4. *Let p , ζ_J , ω be as in Lemma 1, and let R and R_Δ be, respectively, the operators in Eq.(3.8) and Eq.(6.4). Choose $\epsilon > 0$ and $q \geq p$, such that for all $g \in \mathcal{L}^2(\Omega)$*

$$\| \exp\{-\epsilon|\Delta t| \Gamma^q\}g \|_2 \leq \| \exp\{-\omega|\Delta t| \Lambda^p\}g \|_2, \quad (6.5)$$

as postulated in Eq. (6.2). Then, $\| R_\Delta \|_2 \leq \| R \|_2 \leq (1 + |\Delta t| \zeta_J)$, the explicit scheme in Eq. (6.4) is unconditionally stable, and U^n satisfies

$$\| U^n \|_2 = \| R_\Delta^n U^0 \|_2 \leq \exp\{n|\Delta t| \zeta_J\} \| U^0 \|_2, \quad n = 1, 2, \dots, N. \quad (6.6)$$

Proof : Let F be any three dimensional vector $[f, g, h]^T$. Then,

$$\begin{aligned} \| S_{\Delta} F \|_2^2 &= \| Q_{\Delta} f \|_2^2 + \| Q_{\Delta} g \|_2^2 + \| Q_{\Delta} h \|_2^2 \\ &\leq \| Q f \|_2^2 + \| Q g \|_2^2 + \| Q h \|_2^2 = \| S F \|_2^2, \end{aligned} \quad (6.7)$$

on using Eq.(6.2). Hence, $\| R_{\Delta} U^n \|_2 \leq \| R U^n \|_2$, and the result follows from Lemma 2. QED.

Remark 3. As mentioned in Remark 2 and illustrated in Section 7, useful pairs (ϵ, q) in the Laplacian stabilized scheme in Eq.(6.4) are generally found interactively after relatively few trials. In many numerical experiments, typical values satisfy $2 < q < 4$, $10^{-10} \leq \epsilon \leq 10^{-6}$.

LEMMA 5. *Let $W(t)$ be the unique solution of Eq.(3.6). Then, with S_{Δ} and P_{Δ} as in Eq.(6.3), the definitions in Eq.(3.9), and $0 \leq n \leq N$,*

$$\begin{aligned} \| \tau^n \|_2 &\leq 1/2(\Delta t)^2 \| \| G^2 W \| \|_{2,\infty}, \\ \| W^n - S_{\Delta} W^n \|_2 &\leq \epsilon |\Delta t| \| \| P_{\Delta} W \| \|_{2,\infty}, \\ |\Delta t| \| G W^n - S_{\Delta} G W^n \|_2 &\leq \epsilon (\Delta t)^2 \| \| P_{\Delta} G W \| \|_{2,\infty}. \end{aligned} \quad (6.8)$$

Proof : The proof follows from expanding in the orthonormal eigenfunctions of Δ as in the proof of Lemma 3. QED.

Using Lemmas 4 and 5, together with the arguments in Theorems 1 and 2, leads to the following corresponding results for the Laplacian stabilized explicit scheme in Eq. (6.4).

THEOREM 3. *Let p, ζ_J, ω , be as in Lemma 1, and choose $\epsilon > 0$ and $q \geq p$, such that Eq. (6.2) is satisfied. With $\Delta t > 0$, let W^n be the unique solution of Eq.(3.6) at $t = n\Delta t$, and let U^n be the corresponding solution of the forward explicit scheme in Eq. (6.4). If $ER_{\Delta}(t) \equiv U^n - W^n$, denotes the error at $t = n\Delta t$, $n = 0, 1, 2, \dots, N$, then*

$$\begin{aligned} \| ER_{\Delta}(t) \|_2 &\leq e^{t\zeta_J} \| ER_{\Delta}(0) \|_2 + \{ \epsilon (e^{t\zeta_J} - 1) / \zeta_J \} \| \| P_{\Delta} W \| \|_{2,\infty} \\ &+ \{ (e^{t\zeta_J} - 1) / \zeta_J \} \{ \epsilon \Delta t \| \| P_{\Delta} G W \| \|_{2,\infty} + (\Delta t / 2) \| \| G^2 W \| \|_{2,\infty} \}. \end{aligned} \quad (6.9)$$

THEOREM 4. *Let p, ζ_J, ω , be as in Lemma 1, and choose $\epsilon > 0$ and $q \geq p$, such that Eq. (6.2) is satisfied. With $\Delta t < 0$, let W^n be the unique solution of the forward well-posed problem in Eq.(3.6) at $s = T_{max} - n|\Delta t|$. Let U^n be the solution of the backward explicit scheme in Eq. (6.4), with initial data $U(0) = [f_b, g_b, h_b]$ as in Eq.(4.5). If $ER_{\Delta}(s) \equiv U^n - W^n$, denotes the error at $s = T_{max} - n|\Delta t|$, $n = 0, 1, 2, \dots, N$, we have, with δ as in Eq.(4.5),*

$$\begin{aligned} \| ER_{\Delta}(s) \|_2 &\leq \delta e^{n|\Delta t|\zeta_J} + \{ \epsilon (e^{n|\Delta t|\zeta_J} - 1) / \zeta_J \} \| \| P_{\Delta} W \| \|_{2,\infty} \\ &+ \{ (e^{n|\Delta t|\zeta_J} - 1) / \zeta_J \} \{ \epsilon |\Delta t| \| \| P_{\Delta} G W \| \|_{2,\infty} + (|\Delta t| / 2) \| \| G^2 W \| \|_{2,\infty} \}. \end{aligned} \quad (6.10)$$

Analogously to Eqs. (4.4), (4.12), we have the following Corollaries to Theorems 3 and 4.

COROLLARY 1. *In the well-posed forward problem in Theorem 3 with exactly known initial data U^0 , choose $\omega = (\zeta_J)^{1-p}$. Then,*

$$\| ER_{\Delta}(t) \|_2 \leq (\zeta_J)^{-p} (e^{t\zeta_J} - 1) (\epsilon/\omega) \| \|P_{\Delta}W\| \|_{2,\infty} + O(\Delta t), \quad 0 \leq t \leq T_{max}. \quad (6.11)$$

COROLLARY 2. *Let $W(t)$ be the exact solution of the forward well-posed problem in Eq.(3.6). With $\Delta t > 0$, $t = k\Delta t$, let $W^k = W(k\Delta t)$. With known M , δ as in Eq.(4.10), let ζ_J and $\beta(t)$ be defined as in Eq.(4.11). Choose $\omega = (\zeta_J)^{1-p}$, and choose $\epsilon > 0$ and $q \geq p$, such that Eq. (6.2) is satisfied. Let U^k now denote the precomputed backward solution in Theorem 4, evaluated at $t = k\Delta t$. Then,*

$$\begin{aligned} \| ER_{\Delta}(t) \|_2 &\leq (\zeta_J)^{-p} \{ \exp[\zeta_J(T_{max} - t)] - 1 \} (\epsilon/\omega) \| \|P_{\Delta}W\| \|_{2,\infty} \\ &\quad + M^{1-\beta(t)} \delta^{\beta(t)} + O(\Delta t), \quad 0 \leq t \leq T_{max}. \end{aligned} \quad (6.12)$$

6.1. FFT Laplacian smoothing in non-rectangular regions. In rectangular regions Ψ , the Fast Fourier Transform is an efficient tool for synthesizing $(-\Delta)^p$ for positive non-integer p . This was used to advantage in the computational experiment in Section 5. However, as was shown in [3], and will be shown again in Section 10 below, FFT Laplacian smoothing may be feasible for Eq. (3.2) in non-rectangular regions Ω , with zero Dirichlet data on an assumed smooth boundary $\partial\Omega$. Enclosing Ω in a rectangle Ψ , a uniform grid is imposed on Ψ , fine enough to sufficiently well approximate $\partial\Omega$. The discrete boundary $\partial\Omega_d$, consisting of the grid points closest to $\partial\Omega$, is then used in place of $\partial\Omega$. The elliptic operator L is now discretized on Ω using centered differencing. At each time step m in Eq. (6.4), after applying the operator $I + \Delta t G$ to U^m on $\Omega \subset \Psi$, the solution is extended to all of Ψ by defining it to be zero on $\Psi - \Omega$. FFT algorithms are then applied on Ψ to synthesize Q_{Δ} in Eq. (6.1), and produce $U^{m+1} = S_{\Delta}(I + \Delta t G)U^m$, while retaining only the values of U^{m+1} on Ω . This process is then repeated at the next time step.

However, if $\partial\Omega$ needs to be approximated to high accuracy, and/or inhomogeneous data are given on $\partial\Omega$ that cannot be reduced to the homogeneous case, the known or precomputed Laplacian eigenfunctions on Ω should be used to construct S_{Δ} . More accurate discretizations on non uniform grids can also be considered.

7. Nonlinear computational experiment on backward in time reconstruction in thermoelastic plate. While the theoretical developments in Sections 3, 4, and 6, are restricted to linear, autonomous, selfadjoint elliptic operators L , the stabilized scheme in Eq. (6.4) may be applied to more general problems. With Ω the open unit square $0 < x, y < 1$, and $T_{max} = 1.44 \times 10^{-3}$, let L be the nonlinear differential operator defined as follows on functions $z(x, y, t)$ on $\Omega \times (0, T_{max})$:

$$Lz = -0.001s(z)\nabla \cdot \{q(x, y, t)\nabla z\} - 0.01(zz_x + zz_y), \quad (7.1)$$

where

$$s(z) = \exp\{0.005\sqrt{|z|}\} \quad (7.2)$$

$$q(x, y, t) = \exp(10t) \{1 + 2 \sin \pi x \sin \pi y\} \geq 1,$$

NONLINEAR THERMOELASTIC PLATE PROBLEM PARTIALLY SUCCESSFUL BACKWARD RECOVERY

Using input data at positive time T , shown in middle row, explicit scheme marching backward in time seeks to recover true initial data at time 0 , shown in top row. Actually recovered data are shown in last row.

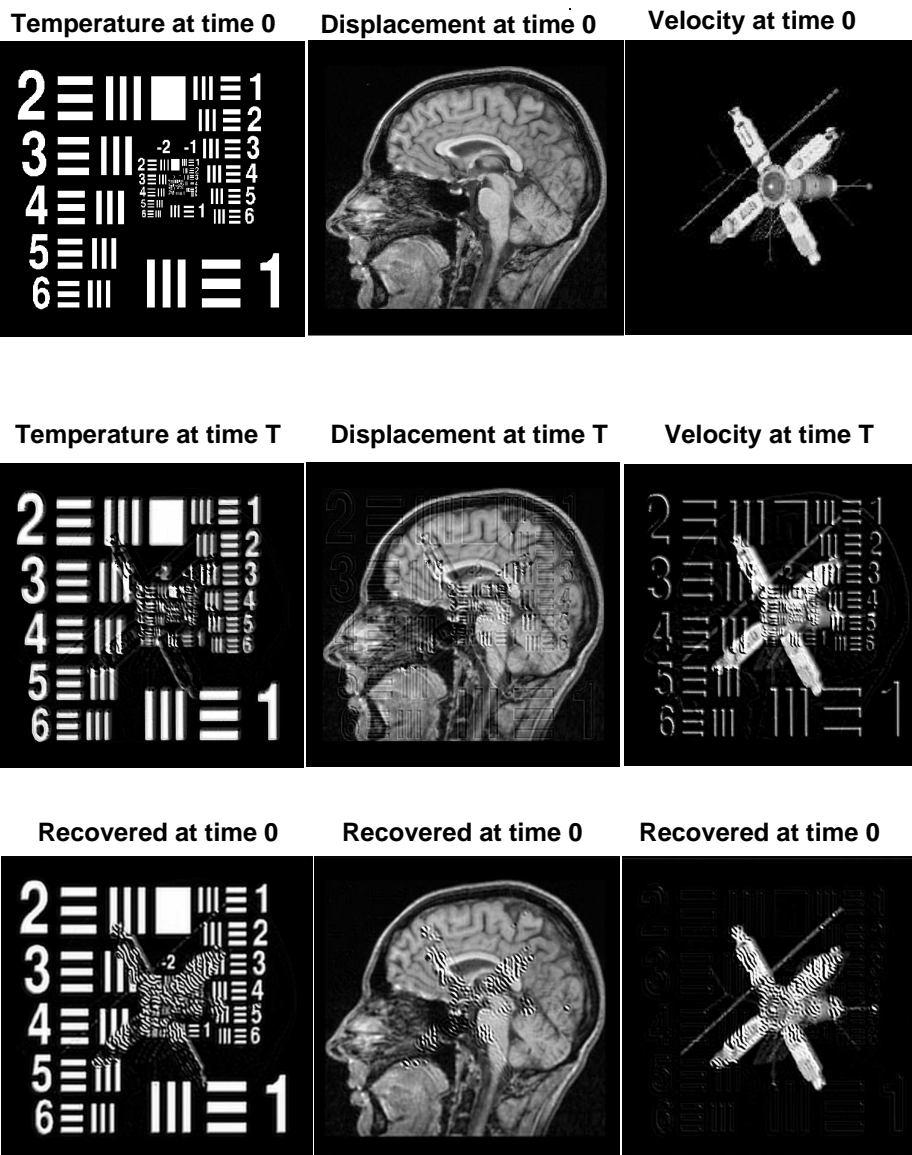


FIG. 7.1. Nonlinear experiment in Section 7 lies outside scope of linear theory developed in Sections 3, 4, and 6, but FFT Laplacian stabilized explicit scheme in Eq. (6.4) can provide useful backward reconstruction, as is evident using image magnification. However, insufficiently accurate input data at T_{max} , coupled with the adverse Hölder continuity in nonlinear backward problems discussed in Section 2, now lead to persistent artifacts in recovered temperature and displacement at $t = 0$.

With $\alpha = \beta = 3$, and $(x, y, t) \in \Omega \times (0, T_{max})$, consider the system

$$\begin{aligned}
 u_t &= -\beta Lu - \alpha Lv, \\
 v_t &= Lw + \alpha Lu, \\
 w_t &= -Lv, \\
 u(x, y, 0) &= f(x, y), \quad v(x, y, 0) = g(x, y), \quad w(x, y, 0) = h(x, y), \\
 u(x, y, t) &= v(x, y, t) = w(x, y, t) = 0, \quad (x, y, t) \in \partial\Omega \times [0, T_{max}].
 \end{aligned} \tag{7.3}$$

This system differs from that considered in Eq. (3.2) in that the operator L is nonlinear, time-dependent, and non-selfadjoint. Therefore, the theoretical developments in Sections 3, 4, and 6, do not apply to Eq. (7.3). In particular, the hypothesis in Eq. (6.2) is not applicable. Nevertheless, backward reconstruction of solutions to Eq. (7.3) can still be attempted using the Laplacian stabilized explicit scheme in Eq. (6.4). The above system is primarily of mathematical interest, and may not reflect any actual physical problem. It is designed to test the robustness of the stabilized explicit scheme in the presence of nonlinearities.

The images used as initial values in the present experiment, shown in the top row of Figure 7.1, are the same as those in Figure 5.1. However, the USAF chart image is now used as the temperature, while the MRI brain image is used as the ‘displacement’. With $\Delta x = \Delta y = 1/512$, a uniform spatial grid was placed on Ω . Using centered finite differencing for spatial discretization, together with $\Delta t = 2.4 \times 10^{-7}$, stable forward computation up to time $T_{max} = 6000\Delta t = 1.44 \times 10^{-3}$, produced the images in the middle row of Figure 7.1. As in Figure 5.1, only the non-negative values, $u^+(x, y, T_{max})$, $v^+(x, y, T_{max})$, $w^+(x, y, T_{max})$, defined in Eq. (5.2), were used to form the middle row images.

On-line image magnification in Figure 7.1 reveals the extent of interaction in these three middle row images. In particular, the MRI brain and satellite images are noticeably affected by the USAF chart image, while the MRI and USAF images appear only mildly affected by the satellite image. The actual computed data $u(x, y, T_{max})$, $v(x, y, T_{max})$, $w(x, y, T_{max})$, exhibit substantial negative values as a natural consequence of the evolution in Eq. (7.3). These data may not be as good an approximation to the true solution, as was the case in Figure 5.1. Only second order accurate centered differencing was used for spatial discretization in Figure 7.1, as compared to the significantly more accurate spectral Fourier discretization method used in Figure 5.1.

The Laplacian stabilized explicit scheme in Eq. (6.4) was applied to the above computed data. Using the previous values of $\Delta x, \Delta y$, together with a six times larger value of $|\Delta t|$, the scheme was used to march 1000 time steps backward from $t = T_{max}$. Here, the ability to perform stable *explicit* computations with a significantly larger $|\Delta t|$, together with the efficient FFT synthesis of the smoothing operator Q_Δ in Eq. (6.2), provides an important advantage in nonlinear ill-posed initial value problems, by allowing fast trial reconstructions in an interactive search for a suitable parameter pair (ϵ, q) in Eq. (6.4). After relatively few trials, the pair $\epsilon = 6.0 \times 10^{-12}$, $q = 3.875$, was located, and resulted in the images shown in the bottom row of Figure 7.1.

Image magnification reveals significant backward recovery in all three bottom row images. In particular, the strong influence of the USAF chart image on the MRI brain

and satellite images, seen in the middle row in Figure 7.1, has now been considerably reduced, and all three images have been noticeably sharpened.

However, both the USAF chart and MRI brain images in the bottom row of Figure 7.1 are affected by a satellite image artifact at the center of the image. That artifact could not be removed by using smaller values of $|\Delta t|$, nor by locating other parameter pairs (ϵ, q) that produce similar sharpening. Thus, backward recovery in the nonlinear system in Eq. (7.3) appears less successful than was the case in the linear system in Eq. (5.1). That is not unexpected. In the linear autonomous selfadjoint system in Eq. (5.1), the Hölder exponent $\mu(t) = t/T_{max}$ as $t \downarrow 0$, as noted in Section 2. Moreover, in Figure 5.1, the computed input data at $t = T_{max}$ more accurately approximates the true solution than is the case in Figure 7.1. In contrast, as illustrated in the explicit example in Section 2.1, and explored more extensively in [35], the fundamental uncertainty in backward reconstruction in the nonlinear system in Eq. (7.3) is likely to be significantly larger, due to the less accurate input data at $t = T_{max}$ in Figure 8.1, coupled with a more rapidly decaying Hölder exponent $\mu(t)$ as $t \downarrow 0$, in Eq. (2.3).

Significantly, in the above nonlinear experiment, substantially more accurate backward recovery can be achieved from computed data at time $t = T_{max}/2$. Evidently, despite the discretization error and the numerical noise, the computed solution at $t = T_{max}/2$, is still a sufficiently good approximation to the exact solution at that smaller value of t , while becoming progressively less accurate as t increases.

In summary, the computational experiment in Section 7 makes two important points. The Laplacian stabilized explicit scheme in Eq. (6.4) can be successfully applied to a limited class of nonlinear problems, for which the ability to choose a larger value of $|\Delta t|$, along with FFT synthesis of Q_Δ , provide a significant advantage. However, regardless of the computational method used, quality backward reconstruction in nonlinear problems generally requires highly accurate input data at the positive time $t = T_{max}$.

8. A stabilized explicit scheme for linear selfadjoint coupled wave and diffusion equations. Much of the preceding theory in Sections 3, 4, and 6, developed for the thermoelastic system in Eq. (3.2), can also be applied to coupled sound and heat flow.

Let Ω be a bounded domain in R^n with a smooth boundary $\partial\Omega$. Let $\langle \cdot, \cdot \rangle$ and $\|\cdot\|_2$, respectively denote the scalar product and norm on $\mathcal{L}^2(\Omega)$. Let L denote a linear, second order, *positive definite* selfadjoint variable coefficient elliptic differential operator in Ω , with homogeneous Dirichlet boundary conditions on $\partial\Omega$. Let $\{\phi_m\}_{m=1}^\infty$ be the complete set of orthonormal eigenfunctions for L on Ω , and let $\{\lambda_m\}_{m=1}^\infty$, satisfying

$$0 < \lambda_1 \leq \lambda_2 \leq \cdots \leq \lambda_m \leq \cdots \uparrow \infty, \quad (8.1)$$

be the corresponding eigenvalues.

With positive constants a, b, d , consider the linear initial value problem on $\Omega \times (0, T]$,

$$\begin{aligned} u_t &= -bLu - dv, \\ v_t &= aLu - aLw, \\ w_t &= v, \\ u(x, 0) &= f(x), \quad v(x, 0) = g(x), \quad w(x, 0) = h(x). \end{aligned} \quad (8.2)$$

When $L = -\Delta$, $a = c^2$, $b = \sigma$, $d = (\gamma - 1)$, the above system reduces to the linearized equations of coupled sound and heat flow discussed in [4], [7], namely, $w_{tt} = c^2\Delta w - c^2\Delta u$, $u_t = \sigma\Delta u - (\gamma - 1)w_t$, with $w = u = 0$ on $\partial\Omega$, where c is the isothermal sound speed, σ is the thermal conductivity, and $1 < \gamma < 2$, is the ratio of specific heats.

The initial value problem Eq. (8.2) becomes ill-posed when the time direction is reversed. We contemplate such time-reversed computations by allowing for possible *negative* time steps Δt in the explicit difference scheme Eq.(8.7) below. With λ_m as in Eq. (8.1), the positive constants a , b , d , and the operator L as in Eq. (8.2), fix $\omega > 0$ and $p > 1$. Given Δt , define ρ , Λ , Q , ζ_m , q_m , as follows:

$$\begin{aligned} \rho &= \{1 + d + d^2 + 2a^2 + 2b + \sqrt{2a^2 + 2b^2}\}, \quad \Lambda = \rho(I + L), \quad Q = \exp(-\omega|\Delta t|\Lambda^p), \\ \zeta_m &= \rho(1 + \lambda_m) > 1, \quad q_m = \exp(-\omega|\Delta t|(\zeta_m)^p), \quad m \geq 1. \end{aligned} \quad (8.3)$$

Let G , S , and P , be the following 3×3 matrices

$$G = \begin{bmatrix} -bL & -dI & 0 \\ aL & 0 & -aL \\ 0 & I & 0 \end{bmatrix}, \quad S = \begin{bmatrix} Q & 0 & 0 \\ 0 & Q & 0 \\ 0 & 0 & Q \end{bmatrix}, \quad P = \begin{bmatrix} \Lambda^p & 0 & 0 \\ 0 & \Lambda^p & 0 \\ 0 & 0 & \Lambda^p \end{bmatrix}. \quad (8.4)$$

Let W be the three component vector $[u, v, w]^T$. We may rewrite Eq. (8.2) as the equivalent first order system,

$$W_t = GW, \quad 0 < t \leq T_{max}, \quad W(\cdot, 0) = [f, g, h]^T. \quad (8.5)$$

As in Section 3, it is instructive to study the following explicit time-marching finite difference scheme for Eq.(8.5), in which only the time variable is discretized, while the space variables remain continuous. With a given positive integer N , let $|\Delta t| = T_{max}/N$ be the time step magnitude, and let W^n denote $W(\cdot, n\Delta t)$, $n = 0, 1, \dots, N$. If $W(\cdot, t)$ is the unique solution of Eq.(8.5), then

$$W^{n+1} = W^n + \Delta t GW^n + \tau^n, \quad (8.6)$$

where the ‘truncation error’ $\tau^n = \frac{1}{2}(\Delta t)^2 G^2 W(\tilde{t})$, with $n|\Delta t| < \tilde{t} < (n+1)|\Delta t|$. With G and S as in Eq.(8.4), let R be the linear operator $R = S + \Delta t SG$. We consider approximating W^n with $U^n \equiv [u^n, v^n]^T$, where

$$U^{n+1} = SU^n + \Delta t SGU^n \equiv RU^n, \quad n = 0, 1, \dots, (N-1), \quad U^0 = [f, g, h]^T. \quad (8.7)$$

With $\Delta t > 0$ and the data U^0 at time $t = 0$, the forward marching scheme in Eq.(8.7) aims to solve a well-posed problem. However, with $\Delta t < 0$, together with *appropriate* data U^0 at time T_{max} , marching backward from T_{max} in Eq.(8.7) attempts to solve an ill-posed problem. Define the following norms for three component vectors such as $W(\cdot, t)$ and U^n ,

$$\begin{aligned} \|W(\cdot, t)\|_2 &= \{\|u(\cdot, t)\|_2^2 + \|v(\cdot, t)\|_2^2 + \|w(\cdot, t)\|_2^2\}^{1/2}, \\ \|U^n\|_2 &= \{\|u^n\|_2^2 + \|v^n\|_2^2 + \|w^n\|_2^2\}^{1/2}, \\ \| \|W\| \|_2, \infty &= \sup_{0 \leq t \leq T_{max}} \{\|W(\cdot, t)\|_2\}. \end{aligned} \quad (8.8)$$

LEMMA 6. With $p > 1$, and ζ_m, q_m , as in Eq. (8.3), fix a positive integer J , and choose $\omega \geq (\zeta_J)^{1-p}$. Then,

$$q_m (1 + |\Delta t| \zeta_m) \leq 1 + |\Delta t| \zeta_J, \quad m \geq 1. \quad (8.9)$$

Proof: This is Lemma 1 in Section 3, with ρ in Eq. (8.3) replacing ν in Eq. (3.3), and hence, a new definition of ζ_m, q_m .

LEMMA 7. With ω, p, ζ_J , as in Lemma 6, and R as in Eq.(8.7), we have $\|R\|_{2 \leq} \leq 1 + |\Delta t| \zeta_J$. The explicit scheme in Eq.(8.7) is unconditionally stable, and

$$\|U^n\|_{2 \leq} = \|R^n U^0\|_{2 \leq} \leq \exp\{n|\Delta t| \zeta_J\} \|U^0\|_{2 \leq}, \quad n = 1, 2, \dots, N. \quad (8.10)$$

Proof: In the system $U^{n+1} = SU^n + \Delta t SGU^n$, expand in the orthonormal eigenfunctions ϕ_m , using $L\phi_m = \lambda_m \phi_m$. Let $u^n = \sum_{m=1}^{\infty} u_m^n \phi_m$, $v^n = \sum_{m=1}^{\infty} v_m^n \phi_m$, $w^n = \sum_{m=1}^{\infty} w_m^n \phi_m$, where $z_m^n = \langle z^n, \phi_m \rangle$. Then, with q_m as in Eq. (8.3),

$$\begin{aligned} u_m^{n+1} &= q_m u_m^n - q_m \Delta t (b \lambda_m u_m^n + d v_m^n), \\ v_m^{n+1} &= q_m v_m^n + q_m \lambda_m \Delta t (a u_m^n - a w_m^n), \\ w_m^{n+1} &= q_m w_m^n + q_m \Delta t v_m^n. \end{aligned} \quad (8.11)$$

Hence,

$$\begin{aligned} |u_m^{n+1}|^2 &\leq q_m^2 |u_m^n|^2 + q_m^2 \Delta t^2 |b \lambda_m u_m^n + d v_m^n|^2 + 2q_m^2 |\Delta t| |u_m^n| |b \lambda_m u_m^n + d v_m^n|, \\ |v_m^{n+1}|^2 &\leq q_m^2 |v_m^n|^2 + q_m^2 \Delta t^2 \lambda_m^2 |a u_m^n - a w_m^n|^2 + 2q_m^2 |\Delta t| \lambda_m |v_m^n| |a u_m^n - a w_m^n|, \\ |w_m^{n+1}|^2 &\leq q_m^2 |w_m^n|^2 + q_m^2 \Delta t^2 |v_m^n|^2 + 2q_m^2 |\Delta t| |w_m^n v_m^n|. \end{aligned} \quad (8.12)$$

Next, using $2xy \leq x^2 + y^2$,

$$\begin{aligned} 2q_m^2 |\Delta t| |u_m^n| |b \lambda_m u_m^n + d v_m^n| &\leq 2q_m^2 |\Delta t| b \lambda_m |u_m^n|^2 + 2q_m^2 |\Delta t| d |u_m^n v_m^n|, \\ &\leq 2q_m^2 |\Delta t| b \lambda_m |u_m^n|^2 + q_m^2 |\Delta t| d |u_m^n|^2 + q_m^2 |\Delta t| d |v_m^n|^2, \end{aligned} \quad (8.13)$$

and

$$q_m^2 \Delta t^2 |b \lambda_m u_m^n + d v_m^n|^2 \leq 2q_m^2 \Delta t^2 b^2 \lambda_m^2 |u_m^n|^2 + 2q_m^2 \Delta t^2 d^2 |v_m^n|^2. \quad (8.14)$$

Likewise,

$$\begin{aligned} 2q_m^2 |\Delta t| \lambda_m |v_m^n| |a u_m^n - a w_m^n| &\leq q_m^2 |\Delta t| \lambda_m |v_m^n|^2 + q_m^2 |\Delta t| \lambda_m |a u_m^n - a w_m^n|^2, \\ &\leq q_m^2 |\Delta t| \lambda_m |v_m^n|^2 + 2q_m^2 |\Delta t| \lambda_m a^2 |u_m^n|^2 + 2q_m^2 |\Delta t| \lambda_m a^2 |w_m^n|^2, \end{aligned} \quad (8.15)$$

and

$$q_m^2 \Delta t^2 \lambda_m^2 |a u_m^n - a w_m^n|^2 \leq 2q_m^2 \Delta t^2 \lambda_m^2 a^2 |u_m^n|^2 + 2q_m^2 \Delta t^2 \lambda_m^2 a^2 |w_m^n|^2. \quad (8.16)$$

Therefore,

$$\begin{aligned} |u_m^{n+1}|^2 &\leq q_m^2 \{1 + (d + 2b \lambda_m) |\Delta t| + 2b^2 \lambda_m^2 \Delta t^2\} |u_m^n|^2 \\ &\quad + q_m^2 \{d |\Delta t| + 2d^2 \Delta t^2\} |v_m^n|^2. \end{aligned} \quad (8.17)$$

$$|v_m^{n+1}|^2 \leq q_m^2 \{2a^2 \lambda_m |\Delta t| + 2a^2 \lambda_m^2 \Delta t^2\} |u_m^n|^2 + q_m^2 \{1 + \lambda_m |\Delta t|\} |v_m^n|^2 + q_m^2 \{2a^2 \lambda_m |\Delta t| + 2a^2 \lambda_m^2 \Delta t^2\} |w_m^n|^2. \quad (8.18)$$

$$|w_m^{n+1}|^2 \leq q_m^2 \{1 + |\Delta t|\} |w_m^n|^2 + q_m^2 \{|\Delta t| + \Delta t^2\} |v_m^n|^2. \quad (8.19)$$

Let $\xi_m^k = |u_m^k|^2 + |v_m^k|^2 + |w_m^k|^2$. Combining Eqs. (8.17), (8.18) and (8.19), we find

$$\begin{aligned} \xi_m^{n+1} &\leq |u_m^n|^2 q_m^2 [1 + \{d + (2a^2 + 2b)\lambda_m\}|\Delta t| + (2a^2 + 2b^2)\lambda_m^2 \Delta t^2] \\ &\quad + |v_m^n|^2 q_m^2 [1 + \{1 + d + (1 + 2d^2)|\Delta t| + \lambda_m\}|\Delta t|] \\ &\quad + |w_m^n|^2 q_m^2 [1 + (1 + 2a^2)\lambda_m |\Delta t| + 2a^2 \lambda_m^2 \Delta t^2] \end{aligned} \quad (8.20)$$

With $\rho = \{1 + d + 2d^2 + 2a^2 + 2b + \sqrt{2a^2 + 2b^2}\}$, and $\zeta_m = \rho(1 + \lambda_m) > 1$, we then have $\xi_m^{n+1} < q_m^2 \{1 + \zeta_m |\Delta t|\}^2 \xi_m^n$. Hence,

$$\left(\sum_{m=1}^{\infty} \xi_m^{n+1}\right)^{1/2} < \sup_{m \geq 1} \{q_m(1 + \zeta_m |\Delta t|)\} \left(\sum_{m=1}^{\infty} \xi_m^n\right)^{1/2}, \quad (8.21)$$

which implies Eq. (8.10) on using Lemma 6. QED

LEMMA 8. Let $W(t)$ be the unique solution of Eq.(8.5). Then, with G , S and P as in Eq.(8.4), the definitions of the norms in Eq.(8.8), and $0 \leq n \leq N$,

$$\begin{aligned} \|\tau^n\|_2 &\leq 1/2(\Delta t)^2 \|G^2 W\|_{2,\infty}, \\ \|W^n - SW^n\|_2 &\leq \omega |\Delta t| \|PW\|_{2,\infty}, \\ |\Delta t| \|GW^n - SGW^n\|_2 &\leq \omega (\Delta t)^2 \|PGW\|_{2,\infty}. \end{aligned} \quad (8.22)$$

Proof: The proof is the same as that in Lemma 3 in Section 3.

THEOREM 5. With $\Delta t > 0$, let W^n be the unique solution of Eq. (8.5) at $t = n\Delta t$. Let U^n be the corresponding solution of the forward explicit scheme in Eq. (8.7), and let p , ζ_J , ω , be as in Lemma 6. If $ER(t) \equiv U^n - W^n$, denotes the error at $t = n\Delta t$, $n = 0, 1, 2, \dots, N$, we have

$$\begin{aligned} \|ER(t)\|_2 &\leq e^{t\zeta_J} \|ER(0)\|_2 + \{\omega(e^{t\zeta_J} - 1)/\zeta_J\} \|PW\|_{2,\infty} \\ &\quad + \{(e^{t\zeta_J} - 1)/\zeta_J\} \{\omega \Delta t \|PGW\|_{2,\infty} + (\Delta t/2) \|G^2 W\|_{2,\infty}\}. \end{aligned} \quad (8.23)$$

Proof: The proof is the same as that in Theorem 1 in Section 4.

As in Theorem 1, we may set $ER(0) = 0$ in Eq. (8.23), and choose $\omega = (\zeta_J)^{1-p}$ in Lemma 6. Eq. (8.23) then reduces to

$$\|ER(t)\|_2 \leq (\zeta_J)^{-p} (e^{t\zeta_J} - 1) \|PW\|_{2,\infty} + O(\Delta t), \quad 0 \leq t \leq T_{max}, \quad (8.24)$$

as was the case for the forward problem error in Eq. (4.4).

In the ill-posed problem of marching backward from given data $U_b = [f_b, g_b, h_b]^T$ at $t = T_{max}$, where

$$\|U_b - W(\cdot, T_{max})\|_2 \leq \delta, \quad \|W(\cdot, 0)\|_2 \leq M, \quad (8.25)$$

we have, using the same proof as in Theorem 2 in Section 4,

THEOREM 6. *With $\Delta t < 0$, let W^n be the unique solution of the forward well-posed problem in Eq. (8.5) at $s = T_{max} - n|\Delta t|$. Let U^n be the solution of the backward explicit scheme in Eq. (8.7), with initial data $U(0) = U_b = [f_b, g_b, h_b]$ as in Eq.(8.25). Let p, ζ_J, ω , be as in Lemma 6. If $ER(s) \equiv U^n - W^n$, denotes the error at $s = T_{max} - n|\Delta t|$, $n = 0, 1, 2, \dots, N$, then*

$$\begin{aligned} \|ER(s)\|_2 \leq & \delta e^{n|\Delta t|\zeta_J} + \left\{ \omega(e^{n|\Delta t|\zeta_J} - 1)/\zeta_J \right\} \|PW\|_{2,\infty} \\ & + \left\{ (e^{n|\Delta t|\zeta_J} - 1)/\zeta_J \right\} \left\{ \omega|\Delta t| \|PGW\|_{2,\infty} + (|\Delta t|/2) \|G^2W\|_{2,\infty} \right\}. \end{aligned} \quad (8.26)$$

As was the case in Eq. (4.12) in Section 4, given M and δ as in Eq. (8.25), we choose $\zeta_J = (1/T_{max}) \log(M/\delta)$, $\omega = (\zeta_J)^{1-p}$, and define $\beta(t) = t/T_{max}$. Eq. (8.26) then reduces to

$$\begin{aligned} \|ER(t)\|_2 \leq & (\zeta_J)^{-p} \{ \exp[\zeta_J(T_{max} - t)] - 1 \} \|PW\|_{2,\infty} \\ & + M^{1-\beta(t)} \delta^{\beta(t)} + O(|\Delta t|), \quad 0 \leq t \leq T_{max}. \end{aligned} \quad (8.27)$$

Therefore, in the coupled sound and heat flow system with autonomous selfadjoint spatial operator L , the stabilized explicit scheme in Eq. (8.7) produces *almost best-possible* results, differing from the fundamental uncertainty $M^{1-\beta(t)} \delta^{\beta(t)}$, only by the stabilization penalty $+ O(|\Delta t|)$ truncation error.

8.1. Using the Laplacian for smoothing when L has variable coefficients. All of the results in Section 6 can be applied to the linear system in Eq. (8.5). With ρ, Λ, Q as in Eq. (8.3), let $\Gamma = \rho(I - \Delta)$. For any real $q > 1$ and $\epsilon > 0$, define $Q_\Delta = \exp\{-\epsilon|\Delta t|\Gamma^q\}$. In domains where closed form expressions for the eigenfunctions of the Laplacian are known, it may be advantageous to use the smoothing operator Q_Δ in lieu of Q in the stabilized explicit scheme in Eq. (8.7). This is feasible for those differential operators L for which the hypothesis in Eq. (6.2) is valid, so that, with appropriately chosen (ϵ, q) , $\|Q_\Delta g\|_2 \leq \|Qg\|_2$, for all $g \in \mathcal{L}^2(\Omega)$ and sufficiently small $|\Delta t|$. When this is the case, Lemmas 4 and 5 in Section 6, together with Theorems 3 and 4, and Corollaries 1 and 2, can be restated so as to apply to the Laplace stabilized explicit scheme in Eq. (8.7). Moreover, as discussed in Section 6.1, and demonstrated in the computational experiment in Section 10 below, it may be possible to use efficient FFT algorithms to synthesize Q_Δ even in problems defined on non-rectangular domains Ω .

9. Computational experiment on backward recovery in linear coupled sound and heat flow. Let Ω be the open unit square $0 < x, y < 2\pi$. With $0 \leq t \leq T_{max} = 0.002$, $a = 6$, $b = 1$, $d = 0.4$, consider the following linear autonomous

BACKWARD RECOVERY IN LINEAR COUPLED SOUND AND HEAT FLOW WITH CONSTANT COEFFICIENTS.

Using input data at positive time T , shown in middle row, explicit scheme marching backward in time seeks to recover true initial data at time 0 , shown in top row. Actually recovered data are shown in last row.

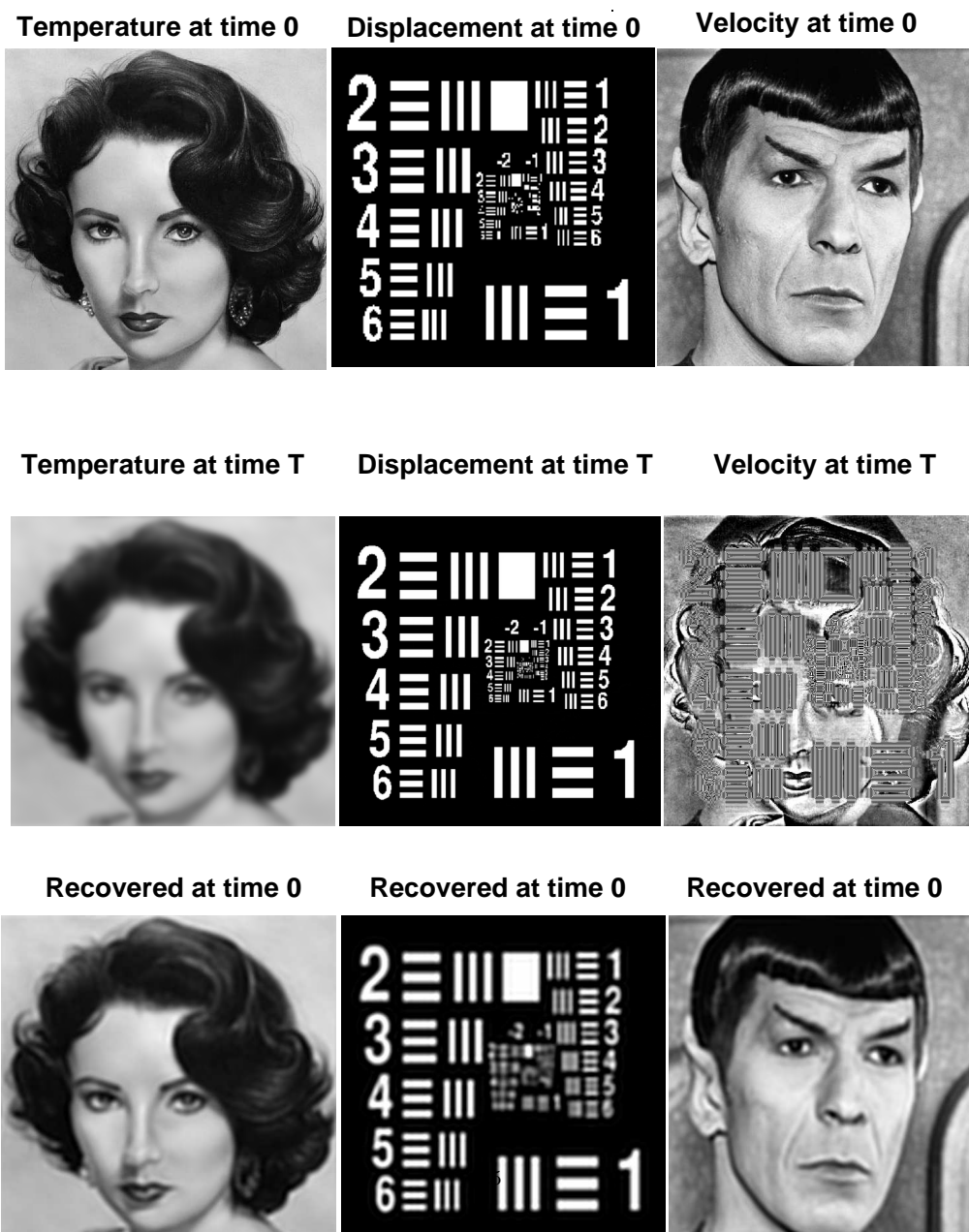


FIG. 9.1. Linear coupled sound and heat flow experiment in Section 9 shows severe distortion and blurring of initial data in forward evolution up to time T_{max} , followed by successful backward in time reconstruction using stabilized explicit scheme in Eq. (8.7).

selfadjoint coupled sound and heat flow system $\Omega \times (0, T_{max})$

$$\begin{aligned}
u_t &= b\Delta u + dv, \\
v_t &= -a\Delta w - a\Delta u, \\
w_t &= v, \\
u(x, y, 0) &= f(x, y), \quad v(x, y, 0) = g(x, y), \quad w(x, y, 0) = h(x, y), \\
u(x, y, t) &= v(x, y, t) = w(x, y, t) = 0, \quad (x, y, t) \in \partial\Omega \times [0, T_{max}].
\end{aligned} \tag{9.1}$$

Here, $u(x, y, t)$ denotes the temperature, $w(x, y, t)$ the displacement, and $v = w_t(x, y, t)$ is the velocity. The initial values $f(x, y)$, $h(x, y)$, $g(x, y)$, are the three 512×512 pixel images shown in the top row of Figure 9.1. The system in Eq. (9.1) differs from that considered in Eq. (5.1) in Section 6. The Laplacian operator is applied to each variable occurring on the right hand side, in each of the three equations in Eq. (5.1), whereas in Eq. (9.1), only the second equation has that property. This leads to a significantly different forward evolution. From the last equation in Eq. (9.1), it is clear that one can expect very little change in the USAF resolution chart image, representing the displacement $w(x, y, t)$, in the forward evolution from $t = 0$ to $t = T_{max} = 0.002$. Likewise, with $d = 0.4$ in the first equation in Eq. (9.1), the forcing term dv can exert almost no influence on the forward evolution of the Elizabeth Taylor temperature image $u(x, y, t)$ up to $T_{max} = 0.002$.

With $\Delta x = \Delta y = (2\pi)/512$, a uniform spatial grid was placed on Ω . Taking advantage of the constant coefficient differential operators in Eq. (9.1), highly accurate spectral Fourier methods for spatial discretization can be used, based on FFT algorithms. With $\Delta t = 1 \times 10^{-7}$, stable forward numerical computation was carried out in Eq.(8.7) up to $T_{max} = 20000\Delta t$. While the initial values f , h , g are non negative functions, the corresponding solution at positive times can develop negative values, as was the case in Figure 5.1. As in that Figure, only the non negative parts $u^+(x, y, T_{max})$, $w^+(x, y, T_{max})$, $v^+(x, y, T_{max})$, as defined in Eq. (5.2), are again displayed as the three images in the middle row of Figure 9.1.

Online image magnification in the middle row in Figure 9.1, indicates that the blurred Elizabeth Taylor image is not visibly affected by the other two images, while the USAF chart image is almost identical to the original in the first row. However, the Mr Spock velocity image has become an unrecognizable mixture of the three images in the first row. In Figure 5.1, each of the three images in the middle row were mixtures of the images in the first row.

Using the computed data $u(x, y, T_{max})$, $w(x, y, T_{max})$, $v(x, y, T_{max})$, and the previous values of Δx , Δy , and Δt , the stabilized explicit scheme in Eq. (8.7) was run backward 20000 time steps from T_{max} . Here, the fact that Ω is a rectangular region with $L = (-\Delta)$, naturally leads to Q_Δ in Section 8.1 as the smoothing operator in Eq.(8.7). This is easily synthesized using FFT algorithms. After very few trials, a pair $\epsilon = 3.0 \times 10^{-10}$, $q = 3.75$, was located, which produced the recovery at $t = 0$ shown in the last row in Figure 9.1.

Evidently, this is a successful reconstruction, owing to highly accurate computed data at $t = T_{max}$, together with a favorable Hölder exponent $\mu(t) = t/T_{max}$, in Eq. (2.3). Note that the recovered USAF chart displacement image is not as sharp as the corresponding image at $t = T_{max}$, due to the blurring caused by Q_Δ .

BACKWARD RECOVERY IN NONLINEAR COUPLED SOUND AND HEAT FLOW IN QUARTER CIRCLE.

Using input data at positive time T , shown in middle row, explicit scheme marching backward in time seeks to recover true initial data at time 0 , shown in top row. Actually recovered data are shown in last row.

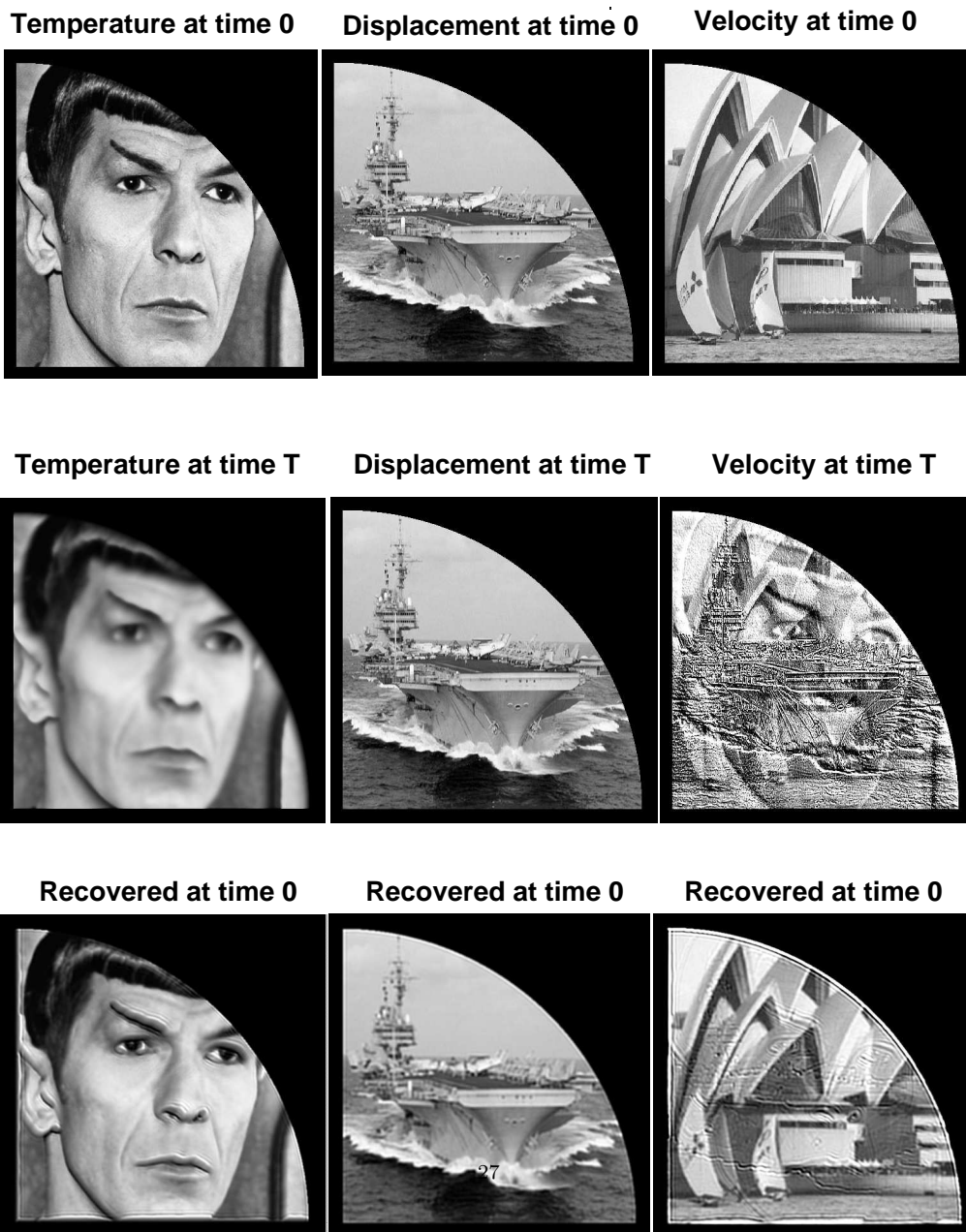


FIG. 10.1. Nonlinear coupled sound and heat flow experiment in Section 10 lies outside scope of linear theory developed in Sections 9 and 10. As discussed in Section 6.1, enclosing quarter circle region Ω in unit square Ψ , allows use of FFT Laplacian smoothing operator Q_{Δ} in backward reconstruction with scheme in Eq. (8.7). Useful backward recovery obtained despite insufficiently accurate input data at time T_{max} .

10. Backward recovery in nonlinear coupled sound and heat flow in non-rectangular region, using FFT Laplacian smoothing. We now highlight the versatility of the stabilized scheme in Eq. (8.7) by considering a nonlinear example in a non-rectangular region. Let Ω be the open quarter circle region in the (x, y) plane,

$$0.05 < x, y < 0.95, \quad (x - 0.05)^2 + (y - 0.05)^2 < (0.9)^2, \quad (10.1)$$

let $T_{max} = 0.002$, and let L be the nonlinear differential operator defined as follows on functions $z(x, y, t)$ on $\Omega \times (0, T_{max})$:

$$Lz = -0.001s(z)\nabla \cdot \{q(x, y)\nabla z\} - 0.01(zz_x + zz_y), \quad (10.2)$$

where

$$s(z) = \exp\{0.005|z|^{0.55}\}, \quad 1 < q(x, y) = \{1 + 2 \sin \pi x \sin \pi y\} \leq 3, \quad (10.3)$$

With $a = 6$, $b = 5$, $d = 0.95$, and $(x, y, t) \in \Omega \times (0, T_{max})$, consider the system

$$\begin{aligned} u_t &= -bLu - dv, \\ v_t &= aLu - aLw, \\ w_t &= v, \end{aligned} \quad (10.4)$$

$$u(x, y, 0) = f(x, y), \quad v(x, y, 0) = g(x, y), \quad w(x, y, 0) = h(x, y),$$

$$u(x, y, t) = v(x, y, t) = w(x, y, t) = 0, \quad (x, y, t) \in \partial\Omega \times [0, T_{max}].$$

As in Section 9, $u(x, y, t)$ denotes the temperature, $w(x, y, t)$ the displacement, and $v = w_t(x, y, t)$ is the velocity. The initial values $f(x, y)$, $h(x, y)$, $g(x, y)$, are the three images shown in the top row of Figure 10.1. Here, the quarter circle region Ω was enclosed in the unit square $\Psi = \{0 < x, y < 1\}$. A 512×512 uniform grid was imposed on Ψ , leading to a discrete boundary $\partial\Omega_d$ consisting of the grid points closest to $\partial\Omega$. This was assumed to sufficiently well-approximate $\partial\Omega$. With $\Delta x = \Delta y = 1/512$, $|\Delta t| = 2.0 \times 10^{-6}$, and homogeneous boundary conditions applied on $\partial\Omega_d$, explicit time differencing, together with centered finite differencing in the space variables, were used in a stable forward computation for $1000\Delta t$. This produced the images at $T_{max} = 0.002$, shown in the middle row in Figure 10.1. Here, the Sydney Opera House velocity image has now become an unrecognizable mixture of the three images in the first row. As in previous experiments, the actual data at T_{max} involve negative values which were not used in forming the middle row images.

While highly accurate spectral Fourier methods were used in Figure 9.1, lower accuracy finite differences were used in Figure 10.1, together with a twenty times larger value of $|\Delta t|$. Consequently, the computed input data at time T_{max} in the middle row of Figure 10.1, are substantially less accurate than was the case in Figure 9.1. Moreover, the linear autonomous selfadjoint theory developed in Section 8, along with the hypothesis in Eq. (6.2), are inapplicable to the nonlinear system in Eq. (10.4). Nevertheless, as discussed in Section 6.1, it is possible to apply FFT-synthesized smoothing operators to stabilize explicit backward in time marching in the present situation.

At each time step m in Eq. (8.7), after applying the operator $(I + \Delta tG)$ to U^m on $\Omega \subset \Psi$, the solution is extended to all of Ψ by defining it to be zero on $\Psi - \Omega$.

FFT algorithms are then applied on Ψ to synthesize Q_Δ in Section 8.1, and produce $U^{m+1} = S_\Delta(I + \Delta t G)U^m$, while retaining only the values of U^{m+1} on Ω . This process is then repeated at the next time step.

With the previous values of $\Delta x, \Delta y, |\Delta t|$, the scheme in Eq. (8.7) with Q_Δ in lieu of Q , was used to march 1000 time steps backward using the computed input data at T_{max} . After very few trials, a parameter pair $\epsilon = 8.0 \times 10^{-11}$, $p = 3.35$, was located, which produced the results in the last row of Figure 10.1. Image magnification reveals useful reconstruction, despite the limited accuracy in the input data at time T_{max} . While faint artifacts remain visible in the recovered Sydney Opera House image, reconstruction of that image from the unrecognizable corresponding image in the middle row, seems remarkable. We have $\alpha T_{max} = 0.012$ in the present experiment, and the nonlinear operator L in Eq. (10.4) differs slightly from that used in the nonlinear experiment in Eq. (7.3), where $\alpha T_{max} = 0.00432$. Thus, forward nonlinear evolution in the middle row of Figure 10.1 has progressed further than was the case in the middle row in Figure 7.1. Nevertheless, higher quality reconstructions were obtained in the present case. As already noted, in contrast to the system in Eq. (10.4), the operator L in Eq. (7.3) acts on every variable on the right hand side of each of the three equations in that system, thereby producing more image mixing and scrambling of data at T_{max} in Figure 7.1, than occurs in Figure 10.1. Hence, coupled sound and heat flow may be more easily run backward in time than thermoelastic wave propagation.

11. Concluding Remarks. The primary aim in this paper was to open doors, and demonstrate the possibility of successful backward reconstruction in a class of problems generally considered intractable. The fact that this was done using explicit marching schemes is especially noteworthy, as such schemes allow the computation of multidimensional nonlinear problems on fine meshes by simply lagging the nonlinearity at the previous time step. Implicit time differencing would necessitate the iterative solution of large nonlinear algebraic systems of difference equations at *every time step*, a formidable and time-consuming task. Such implicit schemes would be impractical in ill-posed reconstruction, where several trial solutions are usually needed prior to locating optimal regularization parameters.

Although the hypothesis in Eq. (6.2) plays an important role, and numerous successful computational experiments appear to validate it, that inequality has not yet been established. The use of Q_Δ in *nonlinear* problems is not contemplated in Eq. (6.2). However, useful results obtained in Figures 7.1 and 10.1, as well as in other nonlinear examples in [1–3], raise interesting research questions.

The use of 512×512 pixel gray scale images as initial data provide challenging test problems, and lead to instructive experiments. Such experiments drew attention to the necessity for sufficient accuracy in the input data at time T_{max} , owing to the fragile Hölder continuity in backward in time continuation with non selfadjoint, or nonlinear, spatial operators.

REFERENCES

- [1] Carasso AS. Stable explicit time-marching in well-posed or ill-posed nonlinear parabolic equations. *Inverse Probl. Sci. Eng.* 2016;24:1364–1384.
- [2] Carasso AS. Stable explicit marching scheme in ill-posed time-reversed viscous wave equations. *Inverse Probl. Sci. Eng.* 2016;24:1454–1474.
- [3] Carasso AS. Stabilized Richardson leapfrog scheme in explicit stepwise computation of forward or backward nonlinear parabolic equations. *Inverse Probl. Sci. Eng.* 2017;25:1–24.

- [4] Richtmyer RD, Morton KW. *Difference Methods for Initial Value Problems*. 2nd ed. New York (NY): Wiley; 1967
- [5] Rouse CA. A method for the numerical calculation of hydrodynamic flow and radiation diffusion by implicit differencing. *J. Soc. Indust. Appl. Math.* 1961;9:127–135.
- [6] Morimoto H. Stability in the wave equation coupled with heat flow. *Numer. Math.* 1962;4:136–145.
- [7] Lattès R, Lions JL. *Méthode de Quasi-Réversibilité et Applications [The Method of Quasi-Reversibility and Applications]*. Paris: Dunod; 1967.
- [8] Lions JL. Sur l'approximation de la solution d'équations d'évolution couplées. *Rend. Mat.* 1968;1:141–176.
- [9] Carasso AS. Coupled sound and heat flow and the method of least squares. *Math. Comp.* 1975;29:447–463.
- [10] Russell DL. A general framework for the study of indirect damping mechanisms in elastic systems. *J. Math. Anal. Appl.* 1993;173:339–358.
- [11] Liu Z, Renardy M. A note on the equations of a thermoelastic plate. *Appl. Math. Lett.* 1995;8:1–6.
- [12] Liu K, Liu Z. Exponential stability and analyticity of abstract linear thermoelastic systems. *Z. Angew. Math. Phys.* 1997;48:885–904.
- [13] Liu Z, Zheng S. *Semigroups associated with dissipative systems*. Chapman and Hall/CRC, New York; 1999.
- [14] Lasiecka I, Triggiani R. Analyticity, and lack thereof, of thermoelastic semigroups. *ESAIM Proceedings* 1998;4:199–222.
- [15] Dell'Oro F, Muñoz Rivera JE, Pata V. Stability properties of an abstract system with applications to linear thermoelastic plates. *Journal of Evolution Equations.* 2013;13: 777–794.
- [16] Tebou L. Stabilization of some coupled hyperbolic/parabolic equations. *Discrete and Continuous Dynamical Systems Series B.* 2010;14:1601–1620.
- [17] Hao J, Liu Z. Stability of an abstract system of coupled hyperbolic and parabolic equations. *Z. Angew. Math. Phys.* 2013;64:1145–1159.
- [18] Benabdallah A, Naso MG. Null controllability of a thermoelastic plate. *Abstract and Applied Analysis.* 2001;7:585–599.
- [19] Avalos G, Lasiecka I. Mechanical and thermal null controllability of thermoelastic plates and singularity of the associated energy function. *Control and Cybernetics.* 2003;32:473–490.
- [20] Miller L. On the cost of fast controls for thermoelastic plates. *Asymptotic Analysis.* 2007;51:93–100.
- [21] Eller M, Lasiecka I, Triggiani R. Exact/approximate controllability of thermoelastic plates with variable thermal coefficients. *Discrete and Continuous Dynamical Systems.* 2001;7:283–302.
- [22] Ames KA, Payne LE. Stabilizing solutions of the equations of dynamical linear thermoelasticity backward in time. *Stability and Applied Analysis of Continuous Media.* 1991;1:243–260.
- [23] Lasiecka I, Renardy M, Triggiani R. Backward uniqueness for thermoelastic plates with rotational forces. *Semigroup Forum.* 2001;62:217–242.
- [24] Koch H, Lasiecka I. Backward uniqueness in linear thermoelasticity with time and space variable coefficients. In *Functional Analysis and Evolution Equations, the Gunter Lumer Volume*, Birkhauser Verlag 2007:389–403. Edited by H. Amann, W. Arendt, M. Hieber, F. Neubrander, S. Nicaise, and J. von Below.
- [25] Ciarletta M. On the uniqueness and continuous dependence of solutions in dynamical thermoelasticity backward in time. *J. Therm. Stress.* 2002;25:969–984.
- [26] Chirita S. On the final boundary value problems in linear thermoelasticity. *Meccanica.* 2012;47:2005–2011.
- [27] Passarella F, Tibullo V, Zampoli V. On the uniqueness in dynamical thermoelasticity backward in time for porous media. *J. Therm. Stress.* 2013;36:501–515.
- [28] Lavrentiev MM. *Some improperly posed problems of mathematical physics*. New York (NY): Springer-Verlag; 1967.
- [29] Ames KA, Straughan B. *Non-standard and improperly posed problems*. New York (NY): Academic Press; 1997.
- [30] Agmon S, Nirenberg L. Properties of solutions of ordinary differential equations in Banach space. *Comm. Pure Appl. Math.* 1963;16:121–239.
- [31] Knops RJ. Logarithmic convexity and other techniques applied to problems in continuum mechanics. In: Knops RJ, editor. *Symposium on non-well-posed problems and logarithmic convexity*. Vol. 316, *Lecture notes in mathematics*. New York (NY): Springer-Verlag; 1973.
- [32] Miller K. Least squares methods for ill-posed problems with a prescribed bound. *SIAM J. Math. Anal.* 1970;1:52–74.

- [33] Miller K. Logarithmic convexity results for holomorphic semigroups. *Pacific J. Math.* 1975;58:549–551.
- [34] Knops R, Payne LE. On the stability of solutions of the Navier-Stokes equations backward in time. *Arch. Rat. Mech. Anal.* 1968;29:331–335.
- [35] Carasso AS. Reconstructing the past from imprecise knowledge of the present: Effective non-uniqueness in solving parabolic equations backward in time. *Math. Methods Appl. Sci.* 2012;36:249-261.
- [36] Babuska I, Osborn JE. Finite element-Galerkin approximation of the eigenvalues and eigenvectors of selfadjoint problems. *Math. Comp.* 1989;52:275-297.
- [37] Heuveline V. On the computation of a very large number of eigenvalues for selfadjoint elliptic operators by means of multigrid methods. *J. Comput. Phys.* 2003;184:321-337
- [38] Platte RB, Driscoll TA. Computing eigenmodes of elliptic operators using radial basis functions. *Comput. Math. Appl.* 2004;48:561-576.
- [39] Morse PM, Feshbach H. *Methods of theoretical physics.* New York (NY): McGraw-Hill; 1953.
- [40] Arendt W, Ter Elst AFM. Gaussian estimates for second order elliptic operators with boundary conditions. *J. Oper. Theory.* 1997;38:87-130.
- [41] Aronson DG. Bounds for the fundamental solution of a parabolic equation. *Bull. Am. Math. Soc.* 1967;73:890-896.
- [42] Ouhabaz EM. Gaussian estimates and holomorphy of semigroups. *Proc. Am. Math. Soc.* 1995;123:1465-1474.
- [43] Ouhabaz EM. Gaussian upper bounds for heat kernels of second order elliptic operators with complex coefficients on arbitrary domains. *J. Oper. Theory.* 2004;51:335-360.